A Monte Carlo Simulation Study on Adsorption of Nitrogen Oxides (NO_x) in zeolites

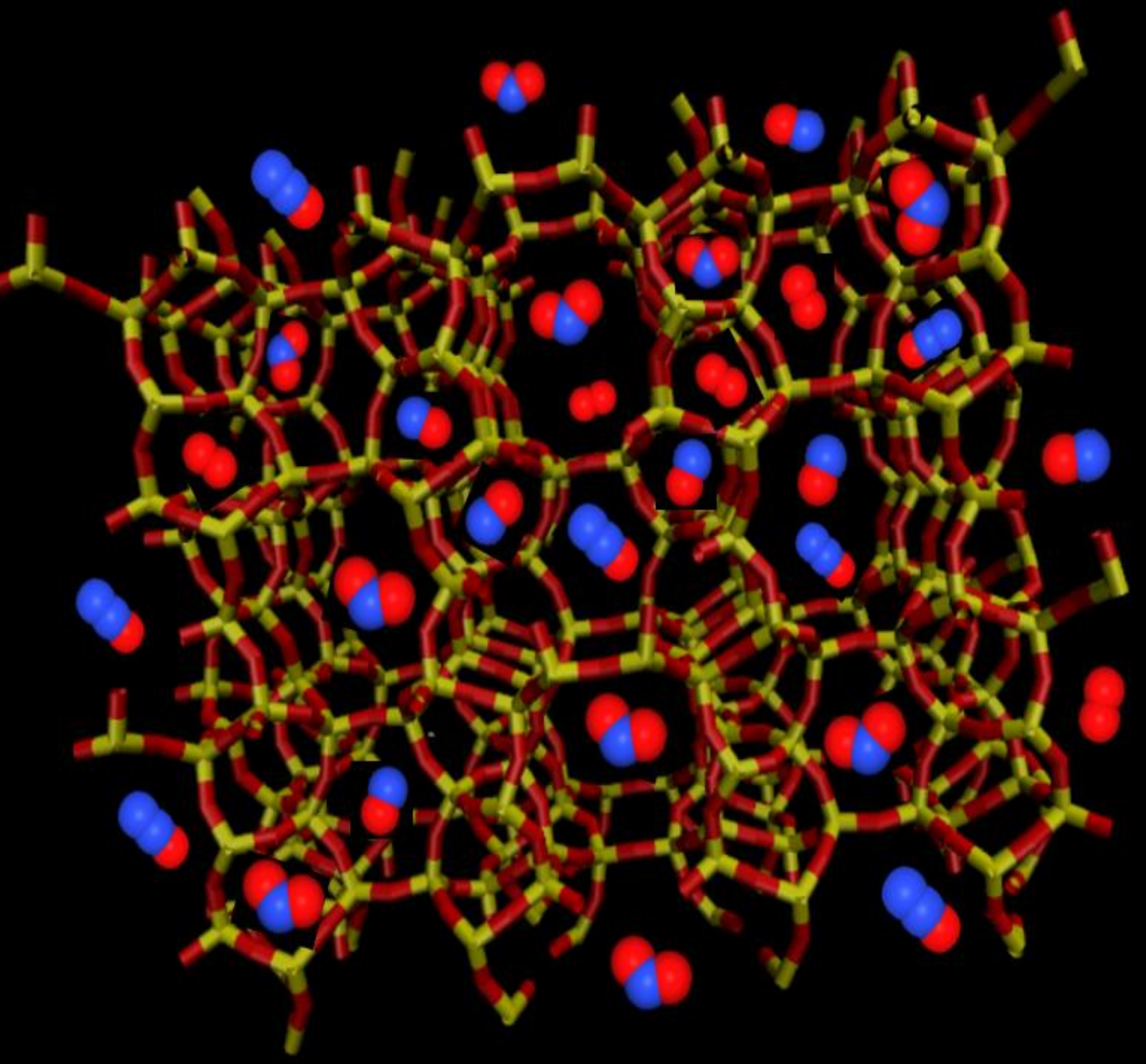

TU Delft

A Monte Carlo Simulation Study on Adsorption of Nitrogen Oxides (NO_x) in zeolites.

by

Grevil Colaco

to obtain the degree of Master of Science

at the Delft University of Technology,

to be defended publicly on Friday June 12, 2020 at 11:00 AM.

Student number:	4713613	
Thesis committee:	Prof. dr. ir. Thijs Vlugt,	TU Delft, chairman
	Dr. Othon Moultos,	TU Delft, supervisor
	Prof. dr. ir. Earl Goetheer,	TU Delft, committee
	Ir. Mate Erdos,	TU Delft, daily supervisor

TU Delft

”You don’t have to be great to start, but you have to start to be great.”

– Zig Ziglar

Abstract

Nitrogen oxides (NO_x) are significant sources of air pollution. Nitrogen oxides like Nitric oxide (NO) and Nitrogen dioxide (NO_2) are mainly responsible for the acid rain and smog. Nitrous oxide (N_2O), also known as the laughing gas, is the major greenhouse gas that is responsible for the ozone layer's damage in the troposphere. According to the Environmental Protection Agency (EPA) report, one pound of N_2O is 300 times more potent greenhouse gas than one pound of CO_2. The significant emitters of Nitrogen oxides (NO_x) are automobiles, agricultural sources, thermal power plants, and chemical processes like Nitric acid production plants, paint manufacturing, etc.

This study mainly focuses on the tail gas emitted from the Nitric acid production facility. The tail gas emitted during the HNO_3 production consists of almost 2% of O_2, 200-400 ppm of NO_2, and NO, whereas 800 ppm of N_2O. As N_2O is the most emitted gas from the Nitric acid production facility, it is followed by NO_2 and NO, so it is essential to reduce these pollutants from the tail gas. Selective catalytic reduction (SCR) is a well-known technique currently involved in reducing NO_x via the adsorption process from the Nitric acid production facility. But the costs involved in these methods are quite high. Nanoporous materials like zeolite exhibit uniform pore size and high thermal stability are said to be the promising adsorbents of NO_x. The availability of a large number of zeolites makes it impossible to identify the proper zeolite for NO_x adsorption experimentally. In such situations, molecular simulations are a powerful tool that can help identify the perfect zeolite. The time and cost involved in the process of molecular simulations are very low.

In this work, Monte Carlo simulations involving reaction ensemble are implemented to obtain the equilibrium composition of NO_x components at desired operating conditions in the Brick molecular simulation package. This is followed by Grand Canonical Monte Carlo simulations (GCMC) and Reactive Grand Canonical Monte Carlo simulations (RXMC-GCMC) for pure and quaternary NO_x gas mixture adsorption in five different zeolites (FAU, FER, MOR, MFI, and TON) using simulation package RASPA. The composition results from the reaction ensemble are validated with the composition results obtained using the Gibbs minimization technique in the MATLAB model, and the results are in good agreement. The quaternary gas mixture adsorption results in five different frameworks from RXMC-GCMC simulations are then validated in Ideal adsorbed solution theory in the Python model, and the results are in good agreement at the given operating conditions.

Acknowledgement

First, I would like to express my utmost gratitude to my supervisor Dr. Othon Moultos, to Chairman Prof.dr.ir.Thijs Vlugt, to committee member Prof.dr.ir.Earl Goetheer and to my daily supervisor Ir. Mate Erdos, for giving such a remarkable opportunity to work on this challenging topic for my Masters Thesis. I also want to thank, Prof.dr.ir.Thijs Vlugt and Dr.Othon Moultos for giving me an opportunity to attend four days RASPA workshop in July 2019 in Wroclaw, Poland. I want to thank Prof.dr.ir.Earl Goetheer for providing the contact of Sitech Services.BV for operating conditions. I want to thank Sitech Services.BV for providing me the operating conditions of the tail gas from the Nitric acid production facility. I also want to express my special gratitude to Ir.Mate Erdos for guiding and helping me during my thesis journey. I want to thank my parents for supporting me during my Masters's studies at TU Delft. Finally, I want to thank my friends for their help, love, and care for me during my master's studies at TU Delft.

Grevil Colaco
Delft, June 2020

Contents

Nomenclature

Acronyms

Å	Angstorm
CCCBD	Computational Chemistry Comparison and Benchmark Data Base
FAU	Faujasite
FER	Ferrierite
JANAF	Joint Army Naval Air Force
MC	Monte Carlo
MD	Molecular Dynamics
MOR	Mordenite
PBC	Periodic Boundary Conditions
PPM	Parts Per Million
GCMC	Grand Canonical Monte Carlo
RXMC	Reaction Monte Carlo

Roman Symbols

ϵ	The well depth and a measure of how strongly the two particles attract each ther
ϵ_0	Vacuum permittivity
Λ	Thermal de Broglie wavelength of the molecule
σ	Symmetry number or rotational symmetry number
$\sigma_{i,j}$	The distance at which the intermolecular potential between the teo particles is zero
Θ_j	Characteristic vibrational temperature of the j^{th} normal mode
Θ_{rot}	Characteristic rotational temperature
ε	Reaction coordinate
D_0	Atomization energy
D_e	The depth of the ground electronic state potential well
f_i	Force on an atom at i^{th} position
g_{e1}	Degeneracy of the electronic
h	Plank constant
k_b	Boltzmann constant
M	Mass of the molecule
m_i	Mass of an atom at i^{th} position
N	Number of particles
P	Pressure
$q(V,T)$	Partition function of ideal gas molecule
$q_{ele}(T)$	Electronic Partition Function
$q_{rot}(T)$	Rotational Partition Function
$q_{trans}(V,T)$	Translational Partition Function
$q_{vib}(T)$	Vibrational Partition Function
$r_{i,j}$	The distance of separation between
T	Temperature
U	Inter-molecular potential between
V	Volume

1

Introduction

Nitrogen oxides (NO_x) are said to be one of the major pollutants that have lead to a significant impact on the atmosphere, human health, and the eviroment[29]. The primary sources of NO_x pollutants are mainly automobiles, airplanes, heavy-duty vehicles, ships, etc. Nitrogen oxides NO_x are also emitted from an industrial and chemical process like power generation, boilers, nitric acid plants, paint manufacturing process and organic chemical nitration process, and also from fuel used in rocket motors[16]. Nitrogen oxides compose of two main components Nitrogen (N_2) and Oxygen (O_2). Nitrogen oxides mainly refers to components like Nitric oxide (NO), Nitrogen dioxide (NO_2) and Nitrous oxide (N_2O) [16]. Nitrous oxide (N_2O) is mainly a non-toxic greenhouse gas, which is mainly emitted from Nitric acid production facility and agricultural sector[24]. Nitric acid production plants are said to be the heavy contributors to nitrous oxide (N_2O). Whereas nitric oxide (NO) and nitrogen dioxide (NO_2) are produced from the combustion process in the IC engines and during the thermal energy production. The supply of excess air for the complete combustion leads to formation of (NO_x)[16][6].

In this work, the main focus is on the (NO_x) components emitted during nitric acid (HNO_3) production from the nitric acid production plant. Here the main concerns are about how we can optimize (HNO_3) production process using Molecular simulations, which will lead to low (NO_x) emission from the tail gas during nitric acid production. Nitrogen oxides (NO_x) components are the main contributors to various atmospheric pollution. Their reaction with VOC's volatile organic compounds, along with the availability of sunlight, leads to the depletion of the ozone layer in the troposphere. The reaction of this (NO_x) components with water vapor in the atmosphere also leads to acid rain. The photochemical reaction caused due to emission of (NO_x) in the atmosphere leads to photochemical smog. Along with this (NO_x) are also toxic to human inhalation and may cause respiratory illnesses[16][13]. (NO_x) and (SO_x) traces in the atmosphere are also responsible for having effects on the carbon capture process. With an increase in pollution and its impact on the environment and human health, its important to put some restrictions on current emissions and look for methods that can help solve this problem. The selective catalytic reduction (SCR), which is the post-combustion technique mainly focusing on the capture of (NO_x), is a fine technique that produces less waste[16]. Currently, ammonia, along with SCR, is used de-NO_x the tail gas emitted from the nitric acid plants[21]. Selective catalytic reduction (SCR) proves to be a good solution, but the cost related to this method is very high[16]. Nanoporous materials like Zeolites prove to be promising sorbents due to their uniform pore size, shape, and thermal stability at high temperatures. These properties make zeolites a better sorbent for capturing, separating, and purifying the

mixture of desired gas components[15]. It is usually a challenge to perform an experimental study and to check which zeolite shows better adsorption of the desired components as this process is quite challenging and consumes lots of time and resources. Molecular simulations are a powerful tool that is widely used to study the adsorption performance of various zeolites and provide a better solution for further experimental studies.

This study mainly focuses on a novel process of adsorption of Nitrogen oxides emitted from the tail gas of Nitric acid production plant in five different zeolites (FAU, FAR, MOR, MFI, TON) using Monte Carlo simulations. The essential goals of this study were to find suitable equilibrium reactions from the literature that includes the vital Nitrogen oxides (NO_2, N_2O, N_2O_4, NO) implemented in this study. Identify the best possible zeolites from the literature for the adsorption of the NO_x components. Select appropriate force fields and the charges for NO_x components and zeolites from the literature. Obtain the operation conditions like pressure, temperature, and composition from the Nitric acid production facility. Calculate the partition function for all the NO_x components and validate the results. Compute the equilibrium composition of the NO_x components in Brick using Reaction Monte Carlo simulations and validate the equilibrium composition results with the Gibbs minimization method. The next step was to obtain the pure component adsorption isotherms in five different zeolites at given operating conditions using Grand Canonical Monte Carlo simulations in RASPA. After this, the goal was to obtain quaternary mixture adsorption isotherm in five different zeolites at given operation conditions using Reactive Grand Canonical Monte Carlo simulation (RXMC-GCMC) in RASPA. And the final step was to validate the adsorption results from the RXMC-GCMC simulations using Ideal Adsorbed Solution Theory.

The operating conditions like pressure, temperature, and the tail gas composition released from the Nitric acid production facility were obtained from a company, Sitech Services. The tail gas was mainly composed of O_2 (1.5% to 2%), N_2O (400 ppm - 800 ppm), NO_2, N_2O_4 and NO around (200) ppm and the rest were the traces of components like CO_2, water vapor and Argon. The tail gas pressure was about 9 to 10 bar, and the temperature was around (480°C - 500°C). Based on the components present in the tail gas like O_2, N_2O, NO_2, N_2O_4, and NO, the equilibrium reactions 3.3, 3.4, 3.5 were taken from the literature. In this study, The temperature and pressure conditions for the simulation of this equilibrium reaction are 10 bar and 773 K. The report is structured in the following way. Chapter 2 discusses the theory of partition functions. The zeolites implemented in this work. Various Monte Carlo techniques like reaction ensemble, Grand Canonical ensemble, and Ideal Adsorbed Solution Theory. Chapter 3 describes the methodology and simulation setup. Chapter 4 focuses on analyzing the results. And chapter 5 discusses the conclusion made and further research.

2

Theory

In this chapter, a brief theory of ideal gas partitions functions, Zeolites implemented in this work, reaction Monte Carlo technique, Grand Canonical Monte Carlo technique, and finally Ideal Adsorbed Solution Theory, are discussed.

2.1. Ideal Gas Partition Function

Partition functions of an ideal gas molecule are important parameters that can be used to calculate various properties such as equilibrium constant, heat capacity, entropy, chemical potential, internal energy, etc. Partition functions can be calculated using data from thermo-chemical tables or by prforming quantum computations [23]. In this study, the Partition Functions were calculated for the molecules involved in this system using the equation from the book by Donald McQuarre and data from CCCBD (Computational Chemistry Comparison and Benchmark Data Base) NIST website [17, 20]. In order, to validate this Partition Function, JANAF (Joint Army Naval Air Force) tables were used [19]. In this chapter, the Partition Functions calculated using equations and from the book by McQuarrie and CCCBD NIST data. The Partition Functions calculated using JANFA tables is demonstrated in section A. The partition function for an Isolated molecule is given by Eq. 2.1

$$q(V,T) = q_{trans}(V,T)q_{rot}(T)q_{vib}(T)q_{ele}(T) \tag{2.1}$$

The terms on the right-hand side of Eq. 2.1 are Translational, Rotational, Vibrational and Electronic Partition Functions. The terms are explained as follows.

2.1.1. Translational Partition Function

The translational part of the partition function is given by the Eq. 2.2 [17, 23].

$$q_{trans}(V,T) = \frac{V}{\Lambda^3} \qquad \Lambda = \frac{h}{\sqrt{2\pi M k_b T}} \tag{2.2}$$

Here, in the Eq. 2.2, Λ is the thermal de Broglie wavelength of the molecule, h is the plank constant, T is the temperature, k_B is the Boltzmann constant and M is the Mass of a molecule [23].

2.1.2. Vibrational Partition Function

The vibrational partition function in Eq. 2.1 for a diatomic molecule is given by Eq. 2.3

$$q_{vib}(T) = \prod_{j=1}^{\alpha} \frac{exp[-\Theta_{vib,j}/2T]}{1 - exp[-\Theta_{vib,j}/T]} \tag{2.3}$$

Here, $\Theta_j = h\nu_j/k_b$ is the characteristic vibrational temperature of the j^{th} normal mode. The values for Θ_j for different molecules can be found from NIST CCCBD data. If the ground vibrational state is considered as zero of energy then the vibrational partition function in Eq. 2.3 can be written as follows [20, 23].

$$q_{vib}(T) = \prod_{j=1}^{\alpha} \frac{1}{1 - exp[-\Theta_{vib,j}/T]} \tag{2.4}$$

2.1.3. Rotational Partition Function

The equation for the rotational partition function for the diatomic and linear polyatomic molecule is the same. This is because the degeneracies and energies for linear polyatomic and diatomic molecules are the same. The expression is given by Eq. 2.5

$$q_{rot}(T) = \frac{T}{\sigma\Theta_{rot}} \tag{2.5}$$

Here σ symmetry number or rotational symmetry number and Θ_{rot} is the characteristic rotational temperature. The symmetry number or rotational symmetry number and Θ_{rot} represents a specific orientation of rigid molecule when identical atoms are interchanged. The values for symmetry number may vary depending on the heteronuclear diatomic or unsymmetrical molecule which is $\sigma = 1$ and for a homonuclear diatomic or symmetrical molecule it is $\sigma = 2$. The symmetry number values for different group of molecules are shown in table 2.1 [20, 23].

Group	σ
C_1, C_i, C_s, $C_{\infty v}$	1
C_n, C_{nv}, C_{nh}	n
$D_{\infty h}$	2
D_n, D_{nh}, D_{nd}	$2n$
S_n	$n/2$
O_h	24
I_h	60

Table 2.1: Symmetry number corresponding to point a group of various molecules. The values in this table are taken from the Computational Chemistry Comparison and Benchmark DataBase (CCCBDB) website [20]

.

The point group in table 2.1 under column one for a molecule can be found on NIST CCCBD website. For example lets consider a molecule of Dinitrogen tetraoxide N_2O_4. For this molecule the corresponding point group is D_{2h} from CCCBD NIST website [20]. If we look at the table 2.1, under group column we can see that for N_2O_4 molecule D_{2h} corresponds to D_{nh}. Here n=2, and for this group the symmetric number σ can be found to be $2n$ and hence for N_2O_4 molecule the value of $\sigma = 4$ [20]. In case of non-linear polyatomic molecule the rotational partition function in the Eq. 2.1 can be written as Eq. 2.6

$$q_{rot}(T) = \frac{\pi^{0.5}}{\sigma}\left(\frac{T^3}{\Theta_{rot,a},\Theta_{rot,b},\Theta_{rot,c}}\right) \tag{2.6}$$

Here, $\Theta_{rot,a},\Theta_{rot,b},\Theta_{rot,c}$ in Eq. 2.6 are rotational temperatures. In case of polyatonic linear or nonlinear molecules there can be more than one values for Θ_{rot}. This values for corresponding molecules can be found on CCCBD NIST website [20, 23].

2.1.4. Electronic Partition Function

For the diatomic and polyatomic ideal gas molecule, the electronic energy to separated atoms at rest in their ground electronic states was considered to be zero. This can be seen in fig. 2.1. Here, D_e is the depth of the ground electronic state potential well[17].

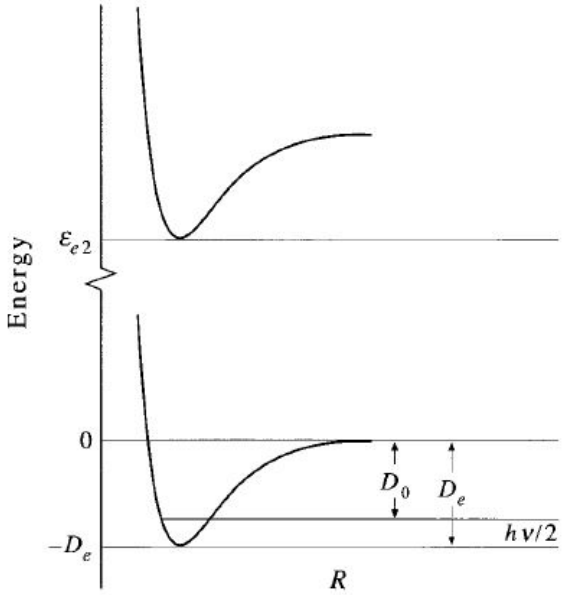

Figure 2.1: The ground and first excited electronic states as a function of the internuclear separation, representing the quantities D_e and D_0 of the ground state and ε_{e2}. [17]

The energy of the ground electronic state is given as $\varepsilon_{e1} = -D_e$. The electronic partition function is given by equation Eq. 2.7 [17].

$$q_{ele}(T) = g_{e1}e^{D_e/k_bT} - g_{e2}e^{-\varepsilon_{e2}/k_bT} \tag{2.7}$$

Here, g_{e1} is the degeneracy of the electronic ground state. The ε_{e2} and D_e values are also shown in fig. 2.1. The difference between the energy of the lowest vibrational state and the dissociated molecule $D_0 = D_e - 1/2h\nu$. D_0 is also called as atomization energy. The values of D_0 for poly and diatomic molecules for this study were taken from chapter 18 in the book by Donald McQuarrie and CCCBD NIST website [17, 20].

2.1.5. Diatomic and Polyatomic Partition Function for ideal gas molecules

In the case of diatomic molecules like $O_{2(g)}$, the ideal gas partition function is given by combination of Eq. 2.2, 2.3, 2.5 and 2.7 [17, 23].

$$q(V,T) = \frac{V}{\Lambda^3}.\frac{T}{\sigma\Theta_{rot}}.\frac{1}{1-exp[-\Theta_{vib,j}/T]}.g_{e1}e^{D_e/k_bT} \tag{2.8}$$

The Polyatomic ideal gas partition function for non-linear molecule is given by combination of Eq. 2.2, 2.4, 2.6 and 2.7 [17, 23].

$$q(V,T) = \frac{V}{\Lambda^3}.\frac{\pi^{0.5}}{\sigma}\left(\frac{T^3}{\Theta_{rot,a},\Theta_{rot,b},\Theta_{rot,c}}\right)\times\prod_{j=1}^{\alpha}\frac{1}{1-exp[-\Theta_{vib,j}/T]}.g_{e1}e^{D_0/k_bT} \tag{2.9}$$

Here α, which is vibrational degrees of freedom, in case of non-linear polyatomic molecule it is given as (3n-6) and for polyatomic linear molecule it is given as (3n-5) respectively.

2.2. Zeolites implemented in this work

In this research, five pure silica zeolite with different geometry and topologies were selected. The selected zeolites were FAU, MFI, MOR, TON, FER. Zeolites deliver excellent flexibility and also favor the higher diffusion of molecules in the structure. All the zeolites used in this study were modeled as a rigid framework as modeled in previous research [23]. The structure, properties, and applications of all five zeolites are mentioned in the subsection below.

2.2.1. Faujasite (FAU)

Faujasite (FAU) has proven to be advantageous in various aspects, such as providing high stability at high temperatures and hydro-chemical conditions. FAU has a 12 member ring window with the size ranging from 0.7-0.8 nm along with 6 and 4 member ring window. FAU exhibits high hydrophobic adsorption selectivity, which makes them favorite for adsorption and catalysis process [35]. FAU has two interconnected cages: the biggest α cage, which is accessible through a 12 member ring window, and the smallest β cage connected via a six-member ring window [23]. FAU zeolites are commonly used for emission control in industrial gas purification. FAU, as a catalyst, is also suitable for fuel liquefaction. Order removal, good hydrocarbon adsorption, and good heat management characteristics are some benefits of FAU zeolite [5]. The top left sub-figure (a) in fig. 2.2 represents the FAU 3D framework representation.

2.2.2. MFI

Zeolites like MFI have provided exceptional catalytic activity and shape selectivity in various petrochemical processes. MFI zeolites have two types of channels in their structure, a straight channel, and a sinusoidal channel. MFI has a ten ring framework, with oxygen atoms responsible for controlling the dimensions of these channels. MFI zeolites are widely used in the automobile industry to control the emission, industrial gas treatment, NO_2, and N_2O reduction [5, 23, 28]. The sub-figure (b) in fig. 2.2 represents the MFI 3D framework.

2.2.3. TON

TON exhibit one-dimensional channel structure of different size and shape. The ten-member rings in TON lead to a limiting diameter of 6.5 and 5 Å. TON zeolites atomic positions were taken from work by B.Marler [2, 14, 23]. The sub-figure (c) in fig. 2.2 represents the TON 3D framework.

2.2.4. Mordenite (MOR)

MOR is considered to have a wide range of applications in the catalytic reactions of hydrocarbons as MOR provides high thermal stability[30]. MOR zeolite is formed by parallel channels in

the z-axis. MOR has extra adsorption sites along the y-axis. The side-pockets in MOR zeolite can be accessed via the main channel only[23]. MOR has two-pore channels, a 12-membered silicon-oxygen ring, main straight channel. And the 8-membered silicon-oxygen ring [30]. The atomic positions for this framework were taken from work by V. Gramlich [9]. The bottom left sub-figure (d) in fig. 2.2 represents the MOR 3D framework.

2.2.5. Ferrierite (FER)

Ferrierite (FER) zeolites have intersected channels with a two-dimensional pore system. FER has a 10 member ring channel of 4.7 Å and 8 member ring channel of 3.4 Å [23]. The crystal dimensionality of FER zeolite causes an impact on various properties and catalytic performance of the zeolite [34]. The bottom right sub-figure (e) in fig. 2.2 represents the FER 3D framework.

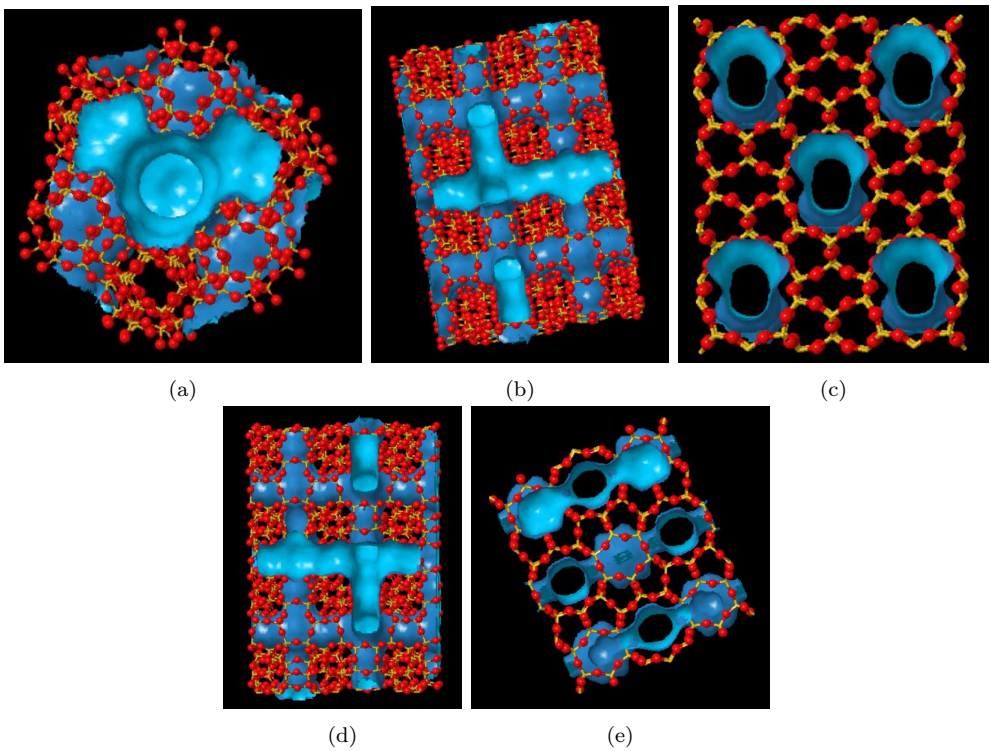

Figure 2.2: Framework representation. The top left sub-figure (a) represents a 3D ball-stick framework display of Si and O_2 atoms in FAU along with the channels system. The top middle sub-figure (b) displays a 3D ball-stick framework display of Si and O_2 atoms in MFI along with the channels system. The top right sub-figure (c) shows the 3D ball-stick framework display of Si and O_2 atoms in TON along with the channels system. The bottom left sub-figure (d) represents 3D ball-stick framework representation of Si and O_2 atoms in MOR along with the channels system, and the bottom right sub-figure (e) represents the 3D ball-stick framework of Si and O_2 atoms in FER along with channels the system. The accessible surfaces of the framework are once in light blue. The surfaces with a darker shade of blue are inaccessible for molecules [1].

2.3. Grand Canonical Monte Carlo simulations (GCMC)

Grand Canonical ensemble or μVT ensemble method is the one in which the Volume (V), the chemical potential μ, and temperature (T) are fixed. But in some cases, the number of particles is allowed to fluctuate. In the case of the gas phase, the gas pressure relates to the chemical potential, and the chemical potential is responsible for the controls of the gas adsorbed in the porous membranes. Let us consider a system of volume V and the number of particles N. The system is combined with a reservoir of volume (V_1-V) and the number of particles (N_1-N). The temperature (T) of the system and the reservoir are at the same[33]. This is represented

in fig 2.3.

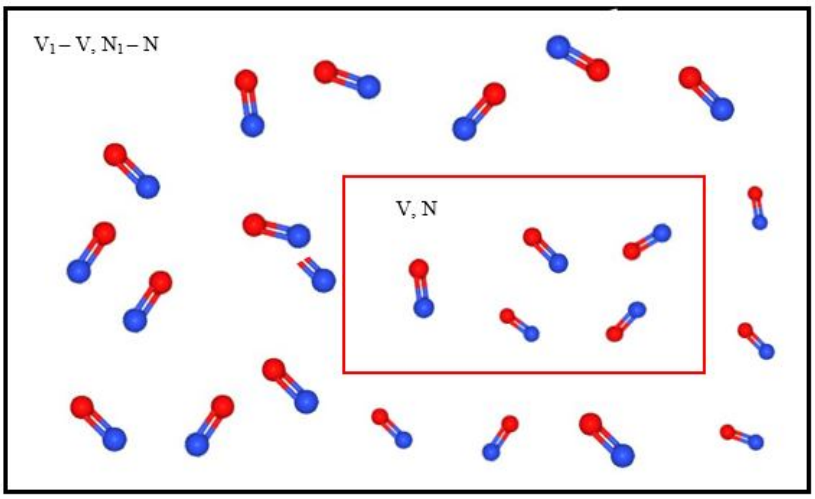

Figure 2.3: The system with the number of particles N and volume V represented by the red box. The reservoir with (N_1-N) particles and volume (V_1-V) represented by the black box.

Here the chemical potential is specified as the reservoir and system exchange number of particles, but the volume does not change. The derivation regarding the acceptance rules of grand-canonical Monte Carlo simulations can be found in the book [33]. Grand Canonical Monte Carlo simulations are widely preferred in the adsorption study of various components in the porous membranes. With the help of GCMC simulations, pure component and multi-component mixture adsorption isotherms can be computed [36]. The detailed GCMC simulation setup for pure and binary component adsorption used in this study is explained in section 3.4.

2.4. Reaction ensemble (RxMC)

Reaction ensemble is a widely used molecular simulation techniques to simulate reaction equilibrium is reaction ensemble [7]. This technique uses a Monte Carlo trial moves to obtain equilibrium distribution of reactants and products. The trial moves used (translation, rotation, etc.) along with additional insert/delete reaction or reaction products. Chemical reactions must be specified first, and the Monte Carlo trial moves are applied on these reactions [23]. In RxMC ensemble only considers thermodynamics and not reaction kinetics [7, 23]. It was reported that RxMC faces some drawbacks with the insertions/deletion of molecules at low temperatures and at higher densities [23]. The improved Reaction ensemble using Continuous Fractional Component Monte Carlo (CFCMC) or (Rx-CFC) method has proved to be more efficient for various applications [7, 23]. (Rx/CFC) the technique requires ideal gas partition function as an input for various reactants and products involved in the reaction. Rx-CFC methods introduce an extended variable called λ, which acts as a coupling parameter for every component involved in the reaction. Let's consider a reaction,

$$2\,NO + O_2 \rightleftharpoons 2\,NO_2 \tag{2.10}$$

The Reaction 2.10 is performed along extended variable λ from 0 to 1. Here 0 denotes full (2NO + O_2) reactants state for fractional components and 1 denotes full product ($2NO_2$) fractional state. The reaction is performed gradually for each component using fractional molecules for each component [7]. In addition to thermalization moves (translation, rotation, etc.), λ moves

are also implemented with three possible outcomes as follows: 1) when λ is between 0 and 1. In this case, the value of lambda changes, but the position and orientation of other molecules are fixed. 2) λ goes to 1. In this case, the number of molecules is kept constant. A trial move is performed to remove a fractional molecule of reactant and insert the fractional molecule of reaction product ($2NO_2$) at randomly selected position and orientation. The position and orientation of other molecules along with λ trial moves are fixed [7, 23]. 3) When λ goes to 0, in this case, the fraction of reactant molecules are transformed into the whole molecule. In contrast, the product molecules that are randomly selected are transformed into a fractional molecule. During this process, the position and orientation of other molecules along with λ moves are kept fixed [7, 23]. The Lambda moves implemented in (Rx/CFC) method are shown in fig 2.4.

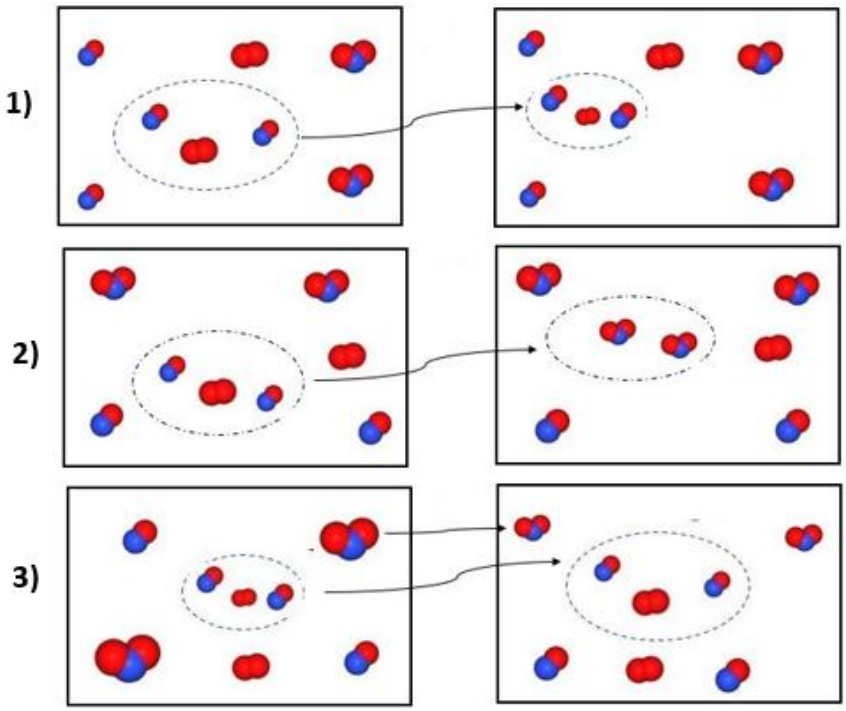

Figure 2.4: The Lambda moves implemented for the reaction 2.10. 1) At the top box, the values of λ are between 0 and 1. The positions and orientations of all other molecules are fixed. Only the interactions of the reactants are scaled. 2) At middlebox λ goes to 1. Here the fractional molecules of the reactants are removed, and the fractional molecules of reaction products are inserted. The positions and orientations of other molecules are kept fixed. 3) At the bottom box, when λ goes to 0, the fractional molecules of the reactants are transferred into whole molecules, and randomly selected reaction products are transformed into fractional molecules[23].

For more detailed derivation and explanation about Reaction ensemble using Continuous Fractional Component Monte Carlo (CFCMC) please look at following reference [7, 11, 23].

2.5. Ideal Adsorbed Solution Theory (IAST)

Ideal adsorbed solution theory (IAST) is a great technique that predicts adsorption isotherms behavior for a multi-component mixture based on pure component adsorption isotherm at desired temperature and pressure conditions. This technique has proved to be a quite effective and powerful way to reduce the need for laborious mixed-gas adsorption measurements. Also, for molecular simulations, simulating an isotherm for a pure component, by implementing IAST

can be faster than performing simulations for multi-component mixture adsorption isotherms in GCMC. IAST implements a python package to perform py.iast in order to calculate and predict isotherms for multi-component mixture in porous medium [26]. pyIAST can fit various standard analytical models for computing isotherms, for example, (Langmuir, Quadratic, approximated Temkin isotherm, Henrys law) to compute a pure-component isotherm. PyIAST can interpolate the data for various pure component isotherm and perform IAST calculations. This evades the time for finding an appropriate analytical model. More information about Ideal Adsorbed Solution Theory (IAST) can be found in reference [26].

3

Methodology & Simulation Setup

The framework and molecular models, along with their partial charges and Lennard-Jones potential, are described. Next, the reaction ensemble setup in brick is described. This is followed by the GCMC setup for the pure component adsorption simulation in RASPA. Then RXMC-GCMC setup for quaternary gas mixture adsorption in RASPA is described. And Last the set up for validation of RXMC-GCMC quaternary gas mixture adsorption isotherms using ideal adsorbed solution theory is explained.

3.1. Framework and Molecular Models along with their Partial Charges and Lenard-Jones Potential

The frameworks used in this study, FAU, FER, MOR, MFI, and TON, were taken from the previous for similar molecular models[16, 29]. All five pure silica zeolites with different geometries and topologies were considered, and all the frameworks were modeled as a rigid framework, as stated in the previous works[16, 29]. MFI zeolites consist of interconnected channels with different directionalities. MFI zeolites with the configuration of the 10-member ring have main channels in the x-axis, which are intersected by zig-zag secondary channels, which leads to a 3-dimensional system with limiting diameters of 4.5 Å – 4.7 Å[16, 29]. For this study, the crystallographic positions of the atoms of MFI zeolite were obtained from the work of H.Van Koningsveld[32]. MOR zeolite structure consists of parallel channels in the z-axis with additional adsorption sites in the y-axis. The channels in MOR, in this study, has 12 member ring windows resulting in 6.5 Å limiting diameter, and the side pockets in MOR are accessible via the main channel only for small molecules. For MOR, crystallographic positions of the atoms for this work were taken from the work by Gramlich[9, 16]. TON zeolite structure has a one-D channel system with 10-member rings, resulting in the limiting diameter of 5 Å. The atomic positions of TON zeolite were taken from the study by Marler[14, 16]. FER zeolite structure has a 2-dimensional intersected channel system with 10-member rings window in z-axis of 4.7 Å and a 8-member rings window in y-axis of 3.4 Å[16]. For this work, the crystallographic positions of the atoms of FER zeolite were taken from the work of R.E.Morris[18]. FAU zeolite structure has a cubic cell with two types of interconnected cages, namely the α-cages, the biggest cages that are accessible through a 12-member ring window, and the smaller ones the β-cages, that are connected by 6-member ring windows. But, the reported narrow windows make these cages inaccessible for most of the molecules that connect them with the 4-member of rings the α-cages[16, 29]. The crystallographic positions of the atoms of FAU zeolite were obtained from the work of J.J.Hriljac[12].

To comply with the experimental conditions, the cavities that are not accessible to the molecules under study need to be blocked. The inaccessible cavities in FER and FAU were blocked using Zeo++ software[37]. Blocking pockets that are not accessible to the molecules is quite essential. To achieve this, one needs to supply the radius of N_2O (r=1.65 Å) molecule to Zeo++ software. The Block files obtained from Zeo++ for FAU and FER were implemented during the GCMC pure component and RXMC-GCMC quaternary mixture simulations in RASPA.

3.1.1. Force Fields

The guest molecule's interactions were defined by the point charges and Lennard-Jones potential. For this study, the Lennard-Jones parameters and the partial charges for the adsorbates and the adsorbents were obtained from the literature. The dimer Dinitrogen tetroxide N_2O_4 molecule was modeled as rigid as in previous work[3, 16]. Oxygen O_2 molecule was represented as a rigid three-site model with two sites located at O atoms and the third one at its COM position. That is, a point charge at the center of mass (COM) of the O_2 molecule to maintains the charge neutrality of the atoms[29]. Similarly, NO_2 molecule is modeled as a three-site Lennard-Jones model with one charged interaction site located at each atom[3, 16, 29]. The NO molecule was modeled as a two-site Lennard-Jones model with partial charges assigned on each site[29]. The Nitrous oxide N_2O molecule was modeled as a rigid molecule as in previous work[10]. For this work, the electrostatic interactions were described by Coulombic potentials and the Ewald summation method. The Van der Waals interactions were described by 12-6 Lennard-Jones potentials as represented in Eq 3.1[10, 16].

$$U(r_{i,j}) = 4\epsilon\left[\left(\frac{\sigma_{i,j}}{r_{i,j}}\right)^{12} - \left(\frac{\sigma_{i,j}}{r_{i,j}}\right)^{6}\right] + \frac{q_i q_j}{4\pi\epsilon_0 r_{ij}} \tag{3.1}$$

The cross interactions were calculated by the Lorentz–Berthelot mixing rules, which are represented by Eq 3.2[10, 16].

$$\sigma_{ij} = \frac{1}{2}(\sigma_{ii} + \sigma_{jj}), \qquad \epsilon_{ij} = \sqrt{\epsilon_{ii}\epsilon_{jj}} \tag{3.2}$$

The point charges and the Lennard-Jones potential for framework atoms were taken from the TraPPE-zeo forcefield[2, 16]. Table 3.1 represents the Lennard-Jones parameters and partial charges of the adsorbates and the adsorbents implemented in this work.

Atoms	$\epsilon/k_b(K)$	σ (Å)	q_i (e)
$N(NO_2)$ [16, 29]	50.36	3.24	0.146
$O(NO_2)$ [16, 29]	62.51	2.93	-0.073
N(NO) [10, 29]	79.5	3.014	0.0288
O(NO) [10, 29]	96.94	2.875	-0.0288
$N1(N_2O)$ [10]	79.167	3.120	-0.3630
$N2(N_2O)$ [10]	27.000	2.800	0.7130
$O1(N_2O)$ [10]	79.000	3.050	-0.3500
$N(N_2O_4)$ [16]	50.36	3.24	0.588
$O(N_2O_4)$ [16]	62.51	2.93	-0.294
O_2 [10, 29]	54.4	3.05	-0.112
O(COM) [10, 29]	0	0	0.224
Si(Zeo) [16]	22	2.30	1.50
O(Zeo) [16]	53	2.30	-0.75

Table 3.1: Lennard-Jones parameters and the partial charges of the molecules and the framework.

3.2. Reaction Ensemble Simulation Setup in Brick

The isobaric-isothermal reaction Monte Carlo method (NPT-RXMC) or the NPT-reaction ensemble was implemented to simulate the bulk phase equilibrium reactions 3.3, 3.4, and 3.5 as shown here at constant pressure, temperature and number of molecules, in order to compute the equilibrium mole fraction, of all the five components under study.

$$N_2O_4 \rightleftharpoons 2\,NO_2 \tag{3.3}$$

$$2\,NO + O_2 \rightleftharpoons 2\,NO_2 \tag{3.4}$$

$$3\,NO \rightleftharpoons NO_2 + N_2O \tag{3.5}$$

The reactions were chosen in such a way that all the components involved in the reaction were present in the tail gas composition, and all three reactions were spontaneous and exergonic. All the reactions 3.3, 3.4 and 3.5 studied here are in gas phase. The simulations were performed in simulation package Brick[11]. The detailed simulation setup, which includes the setup of input files like Molecule definition, Setting, Force-fields, and Topology along with essential parameters, is explained in the upcoming subsection.

3.2.1. Molecule Definition File

Each molecule involved in the simulation has to be defined separately, and a separate file should be made for each molecule. In this study, separate files for N_2O, N_2O_4, NO_2, NO, and O_2 were created in Brick. For each input file, for different molecules, some critical parameters need to be defined. Let us consider an example of a NO_2 molecule input file. The first parameter in NO_2 molecule input file is the molar mass of Nitrogen dioxide in (g/mol). This is defined in block one of the NO_2 molecule input file in Brick. In the second block, the geometry of the molecule has to be defined. Here, for example, the first entry is the atom label. For example,

in the case of NO_2 molecule, the atoms "N" and "O" have to be labeled separately. For this work, the molecules were labeled as, for example, NO_2 molecule was labeled as "N_NO_2" and "O_NO_2". The labels in the molecule definition file should match with the labels, for example, in the forcefield.in file. The mismatch in the labels will prompt an error, and the simulations will not proceed. The third, fourth, and fifth entries in the second block are for the x,y, and z coordinates of the atom. It is important to define the atomic coordinates. For this study, all the atomic coordinates for N_2O, N_2O_4, NO_2, NO and O_2 were taken from NIST CCCBD website[20]. The third block defines atomic bonds. It is vital to define the number of bonds the atoms share in a molecule. The fourth and fifth blocks define bendings and torsions in a molecule. All the molecules involved in this study were modeled as rigid, and hence, bendings and torsions were set to zero. All the molecules were modeled in a similar way, and more information regarding the molecule definition file can be found here[11].

3.2.2. Settings File

The setting.in file consists of critical operating parameters. The most important operating parameters like temperature and pressure are specified in the first block of settings.in file. For the implemented simulations, the operating temperature varied from 273 K -2073 K, and the operating pressure was 1 bar and 10 bar. The units in case of temperature have to be in kelvins. Whereas in case of pressure wide range of units can be specified (kPa, pa, bar, Mpa, etc.). There is also an option for reduced units; in my case, it was set to false as all the units used and set during the simulation were conventional. The Nbox or the number of simulation boxes used during the simulation has to be specified. This parameter is also present in the first block. For all the simulations, Nbox was set to one. The second block in settings.in file contains Nproduction, Nequilibrate, and Ninitialize cycles. During the simulations, the number of production cycles was set to 500,000, and the number of equilibration cycles was set to 100,000, whereas the number of initialization cycles was set to 100.

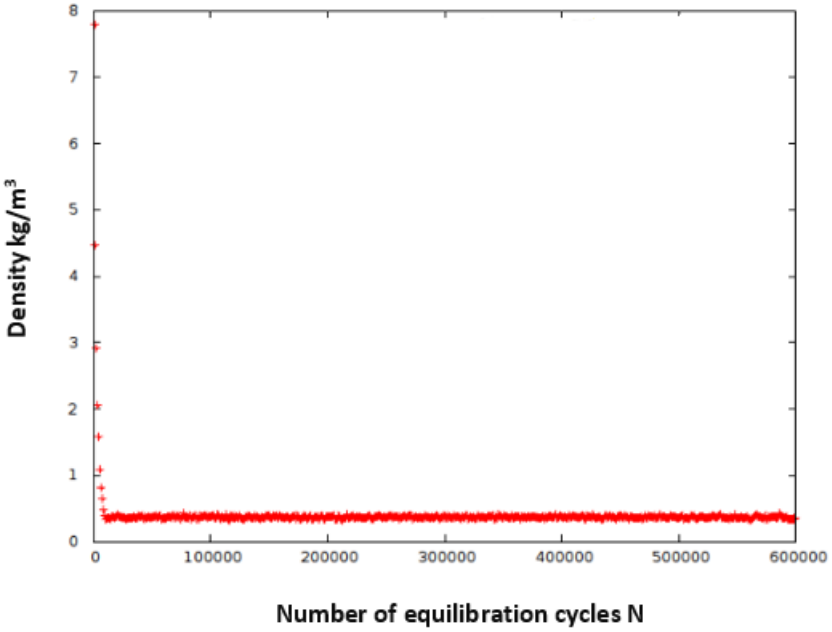

Figure 3.1: Plot for density vs equilibration cycles. The red points represents how well a component is equilibrated in the system befoer the production cycle begins.

It is important to check if your system is well equilibrated before the production cycles start. For example figure 3.1 represents density vs the number of equilibration cycle plot for a single component involved in an RXMC simulation. It can be observed from figure 3.1, the density of a component involved in the simulation is well equilibrated before the commencement of production cycles. If the red points in figure 3.1 show large distortions or large spikes. It means your system is not well equilibrated, and the number of equilibration cycles needs to be increased.

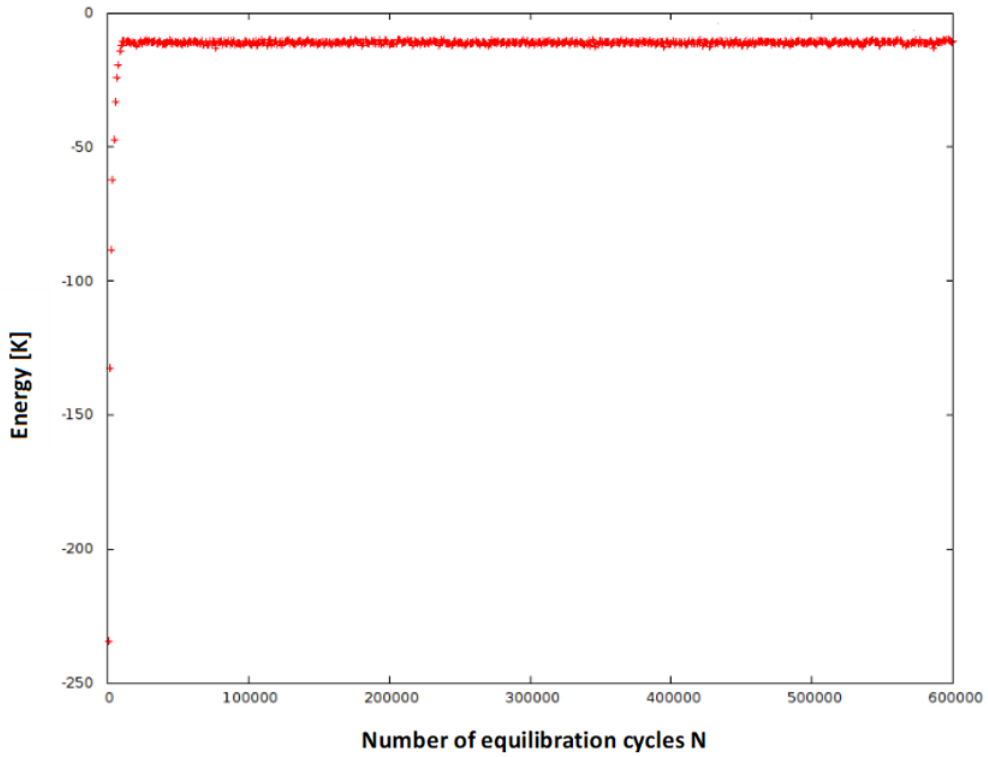

Figure 3.2: Plot for energy vs equilibration cycles. The red line represents how well the energy of a system is equilibrated in before the production cycle begins.

Similarly figure 3.2 represents the equilibration of the energy distribution in the system before the production cycle starts. Lesser the number of spikes in figure 3.2, well, equilibrated is the system. The N in front of the Nproduction, Nequilibrate, and Ninitialize stands for a total number of molecules at the beginning of the simulation, and during the simulation, one cycle constitutes N Monte Carlo steps. It is important to specify at least 20 molecules at the beginning of the simulation. In order to prevent overlaps between the molecules, initialization cycles are quite important, and this can be achieved at the beginning of the simulations, as the initialization cycle performs only translation and rotation moves. The number of equilibration cycles is also important because a well-equilibrated system produces fewer deviations in the results. In the settings.in file (translation, rotation, volume, intramolecular lambda, etc.) moves are also implemented, but for the simulation, the default parameters mentioned in the brick manual have implemented for this moves. More information regarding the settings.in file can be found here[11].

3.2.3. Forcefield File

The file forcefield.in contains the essential set of data that is Lennard-Jones parameters and the partial charges of all the atoms of the molecules available in the reaction as reactants and reaction products during the reaction ensemble simulation. In the first block, the first entry line specifies the number of atom types. For the simulation, the number of atom types was set to 11, as the simulation contained 11 atom types for five different molecules (N_2O, N_2O_4, NO_2, NO, and O_2). The second entry in the first block is atoms. Here the atom of a molecule has to be labeled equivalent to the atoms labels as mentioned in section 3.2. In the same row, the next columns are, the Lennard-Jones parameters, σ in Å and ϵ in K for different atoms of a molecule. The partial charges for different atoms follow this. It is essential to check that the sum of all the charges of the atoms in the file forcefield.in should be zero. This might lead to an error stating, the simulation box is not charge neutral, and the simulations would not proceed when the sum of charges is not zero. In the next columns, the "LJ" (Lennard-Jones) and "EL" (Electrostatic interactions) are represented in terms of boolean values "T" (True) or "F" (False). For example, if an atom doesn't contain any Lennard-Jones parameter, then one has to state in the "LJ" column as "F." This happens mostly in the case of diatomic molecules like O_2 were the common atom is represented as "O_COM" and doesn't contain any Lennard-Jones parameter (see table 3.1). In this work, a similar strategy for "O_COM" atom in the forcefield.in file was implemented. For all the atoms involved in simulations, the Lennard-Jones parameter and partial charges for these atoms were taken from literature, as mentioned in table 3.1.

After defining the atoms, Lennard-Jones parameters, and the partials charges, the energy parameters are defined. The "Cutoff_LJ_Energy," meaning, the Lennard-Jones cut off radius for LJ energy, which by default is 14 Å and for the simulations, the cutoff radius was 14 Å. Similarly, the Cutoff_EI_Energy", meaning, electrostatic interactions energy cutoff radius which by default again is 14 Å, and the same was implemented during the simulations. The energy from the electronic interaction mentioned as "Method_EL_Energy," was calculated using the "Ewald" method. The next energy parameters are the "Alpha_EL_Energy," the energy damping parameter for electrostatic interaction energy method in $Å^{-1}$, and the "Kmax_Ewald," which signifies the number of vector for Ewald method in each direction. The "Alpha_EL_Energy" and the "Kmax_Ewald" parameters are calculated based on box size, which is more than twice the cutoff. In brick, after giving the command "brick calculate Ewald-parameters", the program asks for the box size. After specifying the box size, which was 35 Å, the program displays the output of cutoff, "Alpha_EL_Energy," and the "Kmax_Ewald" parameters. The output for this simulation, the cutoff was 14 Å, and the "Alpha_EL_Energy" value was 0.225533, and the "Kmax_Ewald" value was 8. The remaining parameters were set to default values, as mentioned in the brick manual[11].

3.2.4. Topology File

In this file, some important input parameters like a number of molecules of all the components involved in the reaction need to be defined. The partition functions, which are also an important set of the input parameter and the equilibrium reactions, etc., are also supplied. The first block in topology.in file specifies the number of molecules of different types involved in the reaction. For example, in this simulation, there were five different molecules (N_2O, N_2O_4, NO_2, NO, and O_2). For each of these five components, the number of molecules was specified. During the simulation, 100 molecules were specified to NO, 100 molecules to O_2 and 100 molecules to N_2O_4. For NO_2 and N_2O, zero number of molecules were specified. For simplicity, the molecules were specified only to the reactants in the reaction and not to the reaction products. If you see the equilibrium reactions 3.3, 3.4 and 3.5 you can identify

NO, O_2 and N_2O_4 are the only reactants present in all the three reaction. It was important to check the behavior of mole fractions of all five components at different temperatures (273 K-2073 K) and pressure 1 bar and 10 bar. More about the behavior of mole fractions of all five components at varying temperatures will be discussed in the result section. Make sure the labels of the molecules in topology.in file match with the labels of the molecule definition file.

The second block, in topology.in file is the partition function for an ideal gas. The first entry under the partition function block is the molecule definition. The molecule definition should be the same, as mentioned in section 3.2. Followed by the molecule definition, the next column is the value of the partition function for the corresponding ideal gas molecule. The ideal gas partition functions for all the molecules in this study were calculated using the equations from the book by Donald McQuarrie and data from CCCBD (Computational Chemistry Comparison and Benchmark DataBase) NIST website[17, 20]. To validate the results of the partition functions calculated using the equations from the book by Donald McQuarrie, The calculations of the partition functions using JANAF (Joint Army Naval Air Force) were also performed[19]. For the simulation, the values of the partition function calculated using JANAF tables were used. This is because, as per the suggestions from the previous literature, the values from the partition function calculated using JANAF tables provided good accuracy in results when used as an input to molecular simulations[16]. The partition function for all the Nitrogen oxide (NO_x) components (N_2O, N_2O_4, NO_2, NO, and O_2) implemented in this study were calculated. The values of the partition function computed using the equations from the book, and the JANAF tables are displayed in the result section. While calculating the partition functions by referring to the equations from the book by Donald McQuarrie, one has to maintain caution and use the right equation for diatomic and polyatomic(linear/non-linear) molecule. This simulation system consisted of two diatomic molecules, O_2 and NO. Where NO is a heteronuclear diatomic molecule as it has one "N" atom and one "O" atom. N_2O and N_2O_4 are non-linear polyatomic molecules, and N_2O is a linear polyatomic molecule.

The diatomic partition function in the case of NO and O_2 was calculated using equation 2.8. For polyatomic non-linear molecules, N_2O and N_2O_4, the partition functions were calculated using equation 2.9. N_2O, which is a polyatomic linear molecule, the calculations were performed using equation 3.6.

$$q(V,T) = \frac{V}{\Lambda^3}.\left(\frac{T}{\sigma\Theta_{rot}}\right) \times \prod_{j=1}^{\alpha} \frac{1}{1 - exp[-\Theta_{vib,j}/T]}.g_{e1}e^{D_0/k_bT} \tag{3.6}$$

Here the α represents vibrational degrees of freedom, which in the case of a linear polyatomic molecule is (3n-5), and n is the number of atoms in a molecule. The detailed calculation with an example of the partition functions using equations from the book by McQuarrie and JANAF tables is shown in A. The values of the partition as an input to brick should be in the natural logarithm of partition function times the volume in angstrom (1Å) divided by de Broglie wavelength.

$$ln\left(\frac{q.V}{\Lambda^3}\right) \tag{3.7}$$

A small example of how the partitions function for a nonlinear polyatomic molecule NO_2, calculated using the JANAF table, and using the equations from the book by Donald McQuarrie are shown in section A. The calculated partition function values of all the molecules (N_2O,

N_2O_4, NO_2, NO, and O_2) used as an input to brick are tabulated in section A in table A.1 and A.2.

In the next block, equilibrium reactions are added. The first entry is for the number of reactions. This can vary from 1 to n. where n is the number of reactions. For the simulations, three equilibrium reactions 3.3, 3.4 and 3.5 were implemented. After the number of reactions, it is important to add the components involved in the reaction. Under the column "MolType," one needs to add the molecules, for example, "O_2". Make sure that the label of the molecule matches the label of molecule definition see section 3.2. The next column is "Nstoi," where the stoichiometric coefficient is added. Make sure to add the correct number and do check the stoichiometry of the reaction. Another important thing about adding the stoichiometry coefficient is that in the case of reactants, a negative sign is added before the stoichiometry coefficient, whereas for a product, a positive sign is added in front. For an example consider reaction 3.4. table 3.2

MolType	Nstoic
NO	-2
O_2	-1
NO_2	2

Table 3.2: An example of adding equilibrium reactions in brick.

This is how the reactions were added to the topology.in file in brick. In the next block, the number of the box, which was one, is added, followed by the length and the volume change in cubic meters. All these parameters used during the simulation were default. In the next block, it is essential to add the number of fractional groups, and the maximum displacement for the λ fractional parameter. In this work, there were three fractional groups, whereas the other parameters were set to default. For more information about topology.in file please refer the documentation[11].

3.3. Gibbs Minimization Method Setup in Matlab for Validation of Mole Fraction Computed using Brick

In this section, I will discuss how the mole fractions of all five components (N_2O, N_2O_4, NO_2, NO, and O_2) were computed using Matlab simulation package to validate the mole fractions results from brick simulations. Let us consider a system with a single equilibrium reaction 3.3. In this case, we can easily calculate the composition of the components using equilibrium constant. As the reaction coordinate (ε) can be expressed as a function of mole fraction. Lets consider an example of reaction 3.3. The equilibrium constant K_p is given by equation 3.8

$$k_p = \left(\frac{y_{NO_2}}{y_{N_2O_4}}\right)^{\nu} \tag{3.8}$$

Here ν, is the stoichiometry constant. Whereas the mole fractions of NO_2 and N_2O_4 can be calculated using the equation 3.9

$$y_i = \frac{n_{io} + \sum_j \nu_{i,j}\varepsilon_j}{n_o + \sum_j \nu_j \varepsilon_j} \tag{3.9}$$

Here n_{io} is the initial number of moles of species i and n_o is the total number of moles all the species included in the reaction. y_i is the mole fraction of species i[27]. This looks quite simple

for a single reaction. But when multiple reactions are involved, the system gets quite complicated. The other way of achieving chemical equilibrium is when Gibbs energy is minimum at a given temperature and pressure. Hence a powerful method of Gibbs minimization can be used to determine the composition of the multiple components mixture involved in the reaction. By changing the initial composition, the composition of the products can be obtained as Gibb's energy goes to a minimum. Make sure the number of atoms of each type is kept constant as Gibb's energy is minimized. For ideal gas consideration, the standard Gibbs free energy equals the standard chemical potential at reference pressure one bar and is given by equation 3.10[23, 27].

$$G^{\circ}(T) = \mu^{\circ}(T) = -RTln\left[\left(\frac{q(V,T)}{V}\right)\frac{k_bT}{P^{\circ}}\right] \tag{3.10}$$

We know that for a multi-component mixture the total Gibbs energy is given by equation 3.11

$$G_t = \sum_{i=1}^{S} \mu_i n_i \tag{3.11}$$

Here, S is the total number of components in a mixture. μ_i is the chemical potential of species i and n_i is the number of moles for species i. For the ideal gas consideration the chemical potential is given by equation 3.12[23, 27].

$$\mu_i = \mu^{\circ} + RTln\left(\frac{y_i\varphi_iP}{P^{\circ}}\right) \tag{3.12}$$

Here, φ_i is the fugacity coefficient, and for this simulations, for the ideal gas consideration it is equal to $(\varphi_i = 1)$

From equation 3.11 and 3.12, we can write the total Gibbs energy for multi-component mixture as equation 3.13

$$G_t = \sum_{i=1}^{S} \mu_i^{\circ} n_i + RT\sum_{i=1}^{S} n_i ln\left(\frac{y_i\varphi_iP}{P^{\circ}}\right) \tag{3.13}$$

Once the chemical equilibrium is acquired, the total Gibbs energy for multi-component mixture goes to a minimum, and the minimization is achieved in case of a closed system when the Gibbs energy for multi-component mixture is subjected to material balance, given by equation 3.14[23, 27].

$$A_k = \sum_{i=1}^{S} n_i\alpha_{ik} \tag{3.14}$$

Here A_k is the total number of atoms of type k and α_{ik} is the number of atoms of type k present in component i. After rearranging the terms in the equation 3.14 and equation 3.13, the mole fraction can be calculated using a Matlab toolbox which uses fmincon function for minimization[31]. During my simulations, the components involved in the reaction were added as per the solver requirement. The pressure was defined as 1bar for one simulation and 10 bar for the other. Then the number of moles for all five components was assigned. In my case, 100 moles were assigned to NO, O_2 and N_2O_4, and zero moles were assigned to NO_2

and N_2O. The critical temperature, pressure, and molar mass, along with the acentric factor for all five components, were also defined. The most important parameter, the calculated values of standard reference Gibbs free energy or the standard reference chemical potential, were supplied to code. The calculated values of standard reference Gibbs free energy or the standard reference chemical potential are tabulated in table B.1 in section B.

3.4. Grand Canonical Monte Carlo Simulation Setup for Pure Component Adsorption

Grand Canonical Monte Carlo (GCMC) or μVT method, is a quite popular Monte Carlo method used to study the adsorption of a pure component or multi-component mixture in porous materials. Here, the GCMC simulations setup for adsorption of the pure component in five zeolite membranes (FAU, FER, MOR, MFI, TON) implemented in this study is discussed. The GCMC simulations for pure components was performed at temperature 773 K and pressure ranging from (1-15)bar. Before the simulation setup for the pure components, adsorption is put forth; some prerequisites steps, like computing helium void fraction and blocking inaccessible pockets in zeolites like FAU and FER, have to be considered. All the essential simulation files implemented during the simulation are described here.

3.4.1. Helium Void Fraction

Let's consider a framework, for example, FAU. FAU zeolite consists of some empty spaces. So the void fraction is the empty space in the framework divided by the total volume of the framework. When performing the actual experimentation, helium is used, as helium does not get absorbed in the structure[7]. To compute the helium void fraction for the given framework in RASPA, for example, in FAU, all the essential files like forcefields and mixing rules along with the Lennard-Jones parameters for helium and the framework (see section 3.1.1) are required. The required files like pseudo atom files with the charges for helium and framework atoms (see section 3.1.1). Helium molecule.def file, the FAU framework file with FAU atomic positions, and the simulation input file should be in the same directory. Once all these files are in place, one can simulate to compute the helium void fraction for a given framework. For this simulation, the number of production cycles was set to 250000. The simulations were performed at room temperature of 298 K[7]. The helium void fractions for FAU, MFI, MOR, FER, and TON are tabulated in table 3.3

Framework	Helium void fraction
FAU	0.499061
FER	0.269793
MFI	0.306242
MOR	0.29062
TON	0.187108

Table 3.3: Helium void fractions for FAU, FER, MFI, MOR, TON computed in RASPA

.

3.4.2. Blocking Inaccessible Pockets in FAU and FER Framework

In the case of FAU and FER, there are small pockets that are inaccessible to some molecules. This pocket needs to be blocked. The inaccessible pockets were blocked using software package Zeo++[37]. This is achieved by selecting the molecule with the largest radius. In this study, N_2O molecule was selected, whose radius is 1.65Å. In the software Zeo++, The cif file of the framework needs to be uploaded, for example, the FAU.cif file. Keep in mind, while uploading

the framework.cif file, one has also to provide the radius of the sphere, which in this case is the radius of N_2O molecule. The Zeo++ software passes a sphere of the mentioned radius inside the pockets of the framework and outputs the results about the pockets that are inaccessible to the sphere with a new FAU.block file. The figure 3.3, sub-figure (a) and sub-figure (b) represents the visualization of the blocking pockets process in FAU and FER framework in Zeo++.

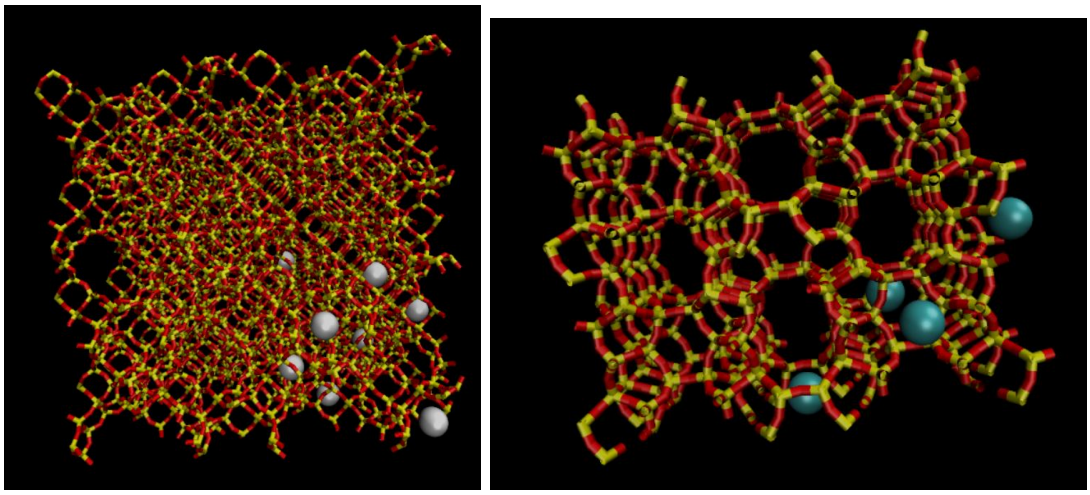

(a) (b)

Figure 3.3: Visual representation of blocking pockets process in FAU and FER zeolites. The white and green sphere in sub-figure a and b represents N_2O molecules that were passed by Zeo++ software inside the FAU and FER framework to block the inaccessible pockets.

This visualization is obtained using visual molecular dynamics software (VMD). To visualize the blocking process, one needs to provide the framework.pdb files from RASPA and framework.block files from Zeo++ software to VMD. In the figure 3.3, sub-figure (a) the white sphere are the N_2O molecules that are passed through FAU framework such that the positions of the inaccessible pockets are obtained, and these pockets are blocked. Similarly the green sphere in the sub-figure (b) in figure 3.3 represents the N_2O molecules passed through the FER framework during the blocking pockets process. This new FAU.block file, along with the FAU.cif file, has to be implemented with some blocking commands in RASPA. For more information please refer to following[7, 37]. The section below describes the necessary file and the setup of these files for the GCMC simulations.

3.4.3. Molecule.def and Framework.cif File

The molecule.def file, for example, (NO_2.def), is a file that contains the atomic position of all the atoms in the molecule along with the bonds and other important parameters like critical temperature, pressure, and acentric factor. In the molecule.def file, in the first block, it is important to specify the critical temperature first in kelvins, followed by the critical pressure in pascal and then the acentric factor. In the second block, the number of atoms in a molecule has to be specified. For example, NO_2 has one "N" and two "O" atoms, which sums up to three atoms. In the next block, it is important to specify, if the molecule is modeled as rigid or flexible. For my simulations, all the molecules were modeled as rigid. In the next block, the XYZ coordinated of the molecules have to be specified. The XYZ coordinates of all the molecules implemented in the study are taken from the NIST CCCBD website[20]. Next is defining the number of bonds the atoms share with other atoms and the bond type. In my simulation file, the NO_2 bonds were two, and the type of bond was rigid. In the case of the

framework.cif files the atomic positions and the files are taken previous studies as mentioned in section 2.2[7].

3.4.4. Force Field and Mixing rule.def File

The force field and mixing rule.def files contain the information regarding Lennard-Jones parameters, frameworks and molecules, tail correction, and mixing rules. In the first block, general rules like truncated vs shifted are applied; during the simulations, the general rule was set to truncated. In the next block, it is essential to specify tail correction, which was set to yes. Then, the number of interactions has to be specified. This can vary, depending on the number of adsorbates and adsorbent atoms involved. For example, for NO_2 molecule along with the MFI framework with the Trappe zeo force field, the number interactions were set to four. In the next block, the interaction type is specified with the atom type, followed by the atom label. For example, "N_NO2". Make sure the atom label matches the label of the molecule.def file. In the next column Lennard-Jons parameters, ϵ in K and σ in Å are entered. The Lennard-Jones parameters implemented during the simulations for adsorbates and adsorbents were taken from literature and are tabulated in table 3.1. In the end, the mixing rules have to be specified. For all the GCMC pure component simulations, Lorentz-Berthelot mixing rules were applied. The information about Force field and mixing rule.def files, can be found here[7].

3.4.5. Pseudo atom.def File

The pseudo atom file contains essential information like partial charges of adsorbates and adsorbents, the mass of atoms, etc. In the first block, the number of pseudo atoms has to be specified. This can vary depending on the number of adsorbates and adsorbents atoms involved. Lets us consider an example form simulation for adsorption of NO molecule in an MFI framework. In this case, NO has two atoms "N" and "O." The MFI framework taken from the previous literature has Si and O atoms. So the total number of pseudo atoms is 4. In the next block, the type of atom followed by the atom label, as mentioned in section 3.4.4 has to be entered for all the atoms involved. Make sure the atom label matches the label of the molecule.def file. In the sixth and seventh columns, followed by the type of atom column, the atomic mass of an atom in (amu) is specified, with the partial charge in the seventh column. The partial charges of all the adsorbates and adsorbents implemented in this study are tabulated in table 3.1. More information about pseudo atom file can be found here[7]

3.4.6. Simulation Input File

The first line of code in the simulation input file specifies the type of simulation, for example, Monte Carlo (MC) or Molecular Dynamics (MD). During the simulations, Monte Carlo was set as a simulation type, which apprises RASPA to start the Monte Carlo part of the simulations. In the next line of code, the number of cycles has to be specified. The number of cycles is the number of production cycles implemented during the simulations. For example, In a Monte Carlo cycles, there are "N" steps, and "N" is the number of Molecules, with 20 steps as a minimum. That means for every molecule involved in every cycle, an MC trial move is performed. This move can be a successful one or a failure. For this simulation, the number of production cycles was set to 500,000. The next line of code specifies the number of cycles for initialization. During this cycle, the position of all the atoms in the system is brought to equilibrium. In the next line, the number of equilibration cycles has to be specified. This line of code makes sure the system is in equilibrium before the production cycle is initiated and helps measure the biasing factors in the system. Fifty thousand cycles were implemented as equilibration cycles during the simulations.

In the next line, loading (as in the presence of framework) and energies during every cycle are printed. The data from my simulations were printed for every 1000 cycles. The next line of code "restart file," states whether to restart the simulations. If set to "yes," it reads the force, positions, and velocities from the restart folder. This line of code is quite useful if the simulations are interrupted. For the case of this simulation, the command was set to "no." In the next line, it is essential to specify the force field. The force fields implemented during the simulation, for all the atoms and framework in the system, were taken from the force field and mixing rule file. The partial charges for all the atoms and framework were taken from the pseudo atom file. In RASPA, there are predefined versions of force fields available. For example, "TraPPE" or "GarciaPerez2006". For all the GCMC simulations for pure component simulations, "local" force fields were implemented. The Van der Waals potentials cutoff was 14 Å. Once the cutoff is specified, all the interactions after the cutoff distance are neglected. Make sure to set the cutoff as half the box length. In the next line of code framework implemented has to be defined, for example, FAU_SI, TON, etc. Make sure to enter the name of the framework, as mentioned in the framework.cif see section 3.4.3. The next line of code defines unit cells in x,y, z-direction. For example, a full cell will consist of these unit cells, and the periodic boundary conditions will be applied on the full cell (the box). Unit cells of (2 2 2) were applied in x,y,z direction during the simulations.

The next line of code specifies whether to remove the atom number from the framework.cif file. For example, "Si1" or "O1". The numbers in front of the atoms are removed such that "Si1", is now represented as "Si." It helps in mapping "Si" and "O" atom charges to the charges provided in the pseudo atom.def file and uses the charges from the pseudo atom.def file. During the simulations "yes" command was specified. In the next line, the helium void fraction has to be specified (see section 3.4.1). Make sure to calculate helium void fraction for the different framework and specify the appropriate value for the appropriate framework. For helium void fraction values of a different framework, refer to table 3.3. Next, the temperature and pressure have to be specified. The temperature was fixed to 773K, whereas pressure varied from (1×10^5 to 15×10^5) pascal. In the next block, the component related parameters like molecule name, definition, and various Monte Carlo trial moves are specified. The molecule's name and definition should match with the molecule.def file labels. For all the simulation, a command "local" was added in front of the molecule definition, as all the molecules were modeled separately and were not taken from RASPA's repository. If the inaccessible pockets need to be blocked, an additional line of code "block pockets" with the command "yes" has to be implemented. The block file name follows this line of code. For example, the inaccessible pockets in the FAU and FER were blocked (see section 3.4.2). Make sure the name of the framework.block file matches with the name entered in front of the "block pocket file name." The trial moves implemented during simulation were (translation, rotation, reinsertion, and swap) probability as implemented in previous research[16]. For more information on simulation input file please refer to the documentation on RASPA[7].

3.5. Reactive Grand Canonical Monte Carlo Simulation Setup for Adsorption of Quaternary Mixture in Zeolites

In this section, the RXMC-GCMC simulation setup for adsorption of a quaternary gas mixture of NO, N_2O, NO_2 and O_2 in FAU, FER, MOR, MFI, TON is described. Most of the file setup required for the simulation is quite similar to GCMC pure component adsorption setup; see section 3.4. The molecule.def file is identical to the file described in section 3.4.3. The most important thing is the molecule.def files for NO, N_2O, NO_2 and O_2 should be in the same directory. The force field and mixing rule.def files are modeled in the same way as described

in section 3.4.4. Caution should be practiced while entering the number of interactions, as for quaternary mixture composition, the number of interactions between adsorbents and adsorbates increases as compared to the interactions in a pure component. The setup for the framework remains the same as mentioned in section 3.4.3. Just an additional framework.block files in the case of FAU and FER need to be added in the simulations files directory. The pseudo atom.def file was modeled in the same way as described in section 3.4.5. Please make sure to add a correct number of pseudo atoms, which will be more than the pure component in the case of the quaternary mixture.

The most important file, the simulation.input, has a similar structure as a pure component simulation input file. For quaternary mixture simulations, the number of production cycles was 500,000, and the equilibration cycles were 50,000. Local force fields for adsorbates and adsorbents were implemented. The force fields and charges for adsorbates and adsorbents were taken from force fields and mixing rule.def and pseudo atom.def files. The cutoff of 14 Å was implemented. The framework implemented for the adsorption process was FAU, FER, MOR, MFI, TON. The unit cells of (2 2 2) were applied in x,y,z direction, as described in section 3.4.6. The command to remove the atom number labels, as mentioned in section 3.4.6, was set to "yes." The value for helium void fraction was added. Make sure to add the correct value of helium void fraction for an identical framework, see section 3.4.1. The temperature was set to 773 K for all the simulations, and the pressure was varied from (1×10^5 to 15×10^5) pascal. In the next line of code component setup and the Monte Carlo, trial moves were implemented. For quaternary mixture adsorption, the components involved were NO, N_2O, NO_2, and O_2. The components were added as component (zero, one, two, three). Make sure the component definition matches with the molecule.def file. Block pockets commands were implemented in the case of FAU and FER zeolites. A new line of code, "mole fraction" was added for all the components. The mole fractions values as an input for RXMC-GCMC simulations for the quaternary mixture were taken from the bulk phase isobaric-isothermal reaction ensemble simulations at 773 K see section 3.2. The mole fraction values are tabulated in the section C in the table C.1 and C.3. For the RXMC-GCMC quaternary mixture simulation, the Monte Carlo trial moves implemented were translation, rotation, reinsertion, identity change, and swap probability. These moves were implemented for all the components involved in the simulation. For more information on quaternary mixture simulation, please refer to the documentation on RASPA[7].

3.6. Ideal Adsorbed Solution Theory (IAST) Setup

The Ideal Adsorbed solution theory model was implemented to predict the quaternary gas mixture adsorption isotherms and, depending on the prediction, validate the GCMC quaternary gas mixture adsorption simulations in RASPA, for all the five frameworks. The same operating conditions, temperature, 773 K, and pressure ranging from (1 bar-15 bar) was implemented. The IAST model setup was done in python, using Jupyter notebook. Any python integrated development environment (IDE) software package can be used for modeling IAST. The first step is installing essential packages in a jupyter notebook. These packages include mumpy, matplotlib, pyiast, and pandas. For better visualization color code, all the components (NO, N_2O, NO_2 and O_2) involved in the process. In the next step, for example, for the MOR framework, the data for pure component loading at 773 K from 1 bar-15 bar pressure from RASPA GCMC simulations was loaded to the jupyter notebook in the form of a csv file. Make sure to upload the data for all the pure components and create a separate data-frame for all the components involved in the process. Do check the data-frame for every component using "df.head()" command to check if correct data was uploaded for the correct component. In the next step, quaternary mixture data is uploaded to the jupyter notebook. The quaternary gas

mixture loading data from RASPA simulations performed at 773 K and 1 bar-15 bar pressure was uploaded in the form of a csv file, and a data-frame for quaternary mixture loading is generated. Again, do cross verify the uploaded data to avoid discrepancies. In my model, most of the data was visualized in the form of plots using the matplotib package.

The next step is the most crucial step where an isotherm for a pure component is computed using the interpolator isotherm pyiast model. The interpolation isotherm uses linear interpolation by interpolating the pure component adsorption data from RASPA GCMC simulations along with the numerical quadrature model to evaluate the integral in order to calculate the spreading pressure as shown in equation 3.15.

$$\pi_i(p_i^\circ) = \frac{RT}{A}\int_0^{p_i^\circ} \frac{n_i^\circ(P)}{P} dP \tag{3.15}$$

Here $\pi_i(p_i^\circ)$ represents spreading pressure, R is the gas constant, p_i° is the pure component gas phase pressure, A is the surface area and $n_i^\circ(P)$ is pure component adsorption at given pressure p[26]. Once the pure component isotherms for all, the components are calculated using "pyiast.InerpolatorIsotherm," the isotherms for each component can be plotted. In the next step, the partial pressure for all the four components is calculated and placed in the form of an array. In the next step, IAST performs component loading for a gas-phase mixture using the data from partial pressure, and the pure component isotherm computed using IAST. The last step is plotting the results and checking if pyIAST prediction matches with the GCMC simulation results. More information about IAST can be found here[26].

4

Results and Discussion

4.1. Results of Blocking Pockets in FAU and FER Zeolites

The results of blocking the inaccessible pockets in FAU and FER zeolites are shown in fig 4.1. The results displayed in figure 4.1 represents the loading of pure N_2O_4 in FER and FAU on the y-axis in mol/kg and pressure ranging from 10^2 to 10^7 pascal on the x-axis. In figure 4.1 the solid orange line with a solid symbol represents pure N_2O_4 loading in mol/kg without blocking the pockets in FER (represented as FER_old). The broken or the dashed orange line in fig 4.1 represents, the pure N_2O_4 loading in mol/kg from literature when inaccessible pockets were blocked in FER (represented as FER_lit)[16].

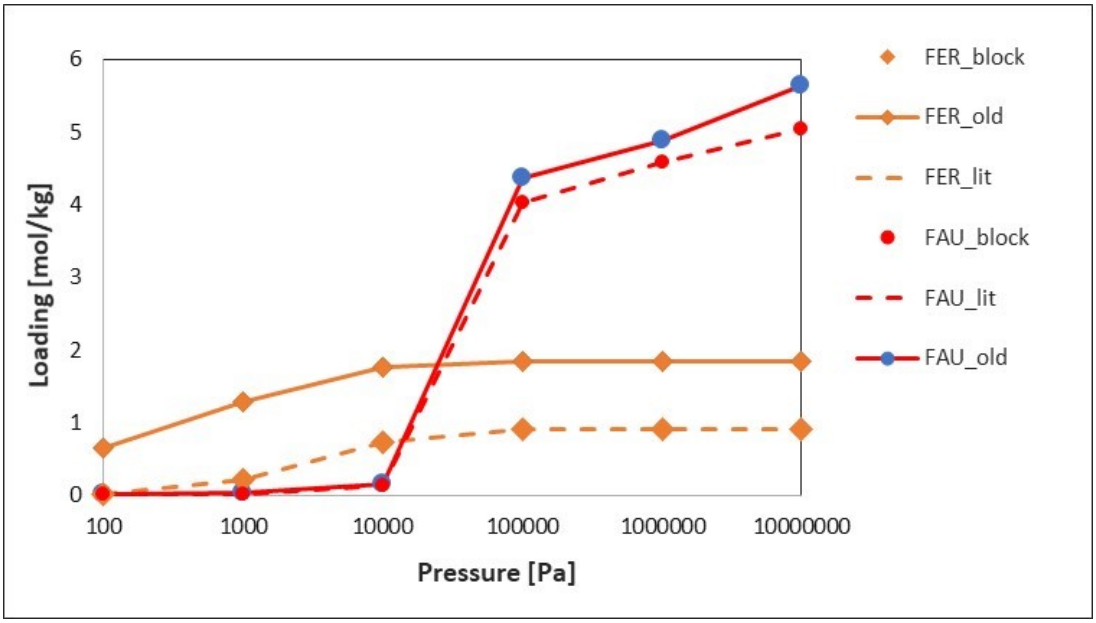

Figure 4.1: The plot for pure N_2O_4 loading in mol/kg vs. pressure in pascal for FER represented in solid orange line (FER_Old) without blocking pockets and dashed line (FER_lit) after blocking pockets (results from the literature), and with the solid orange symbol (FER_block) after blocking pockets in this study. Similarly FAU (represented in the solid red line with blue symbols (FAU_Old) without blocking pockets and the dashed line (FAU_lit) after blocking pockets (results from literature) along with solid red symbol (FER_block)) after blocking pockets in this study.

The solid orange symbol in fig 4.1 are the results for the pure N_2O_4 loading in mol/kg after

blocking pockets in FER zeolite from this study (represented as FER_block). Similarly, the solid red line with solid blue symbols represents pure N_2O_4 loading in mol/kg in FAU without blocking the pockets (represented as FAU_old). The dashed red line (represented as FAU_lit) in fig 4.1 are the pure N_2O_4 loading in mol/kg in FAU from literature, when the pockets were blocked[16]. The solid red symbols (represented as FAU_block) are the pure N_2O_4 loading in mol/kg from this study when inaccessible pockets were blocked. From figure 4.1, it can be noticed the importance of blocking the inaccessible pockets. Results from the literature match quite well with the results from this study, once the pockets in FAU and FER were blocked. It can be seen in fig 4.1, that there is quite a lot of deviation in the FAU_old and FAU_block or FAU_lit results as well as FER_old and FER_block or FER_lit, when the inaccessible pockets are not blocked. Not blocking the pockets in FAU also leads to an increase in simulation time. Without blocking pockets in FAU, it takes more than eight days for a pure N_2O_4 adsorption simulation to complete in RASPA, whereas for FER, there was no significant change in compiling time for pure N_2O_4 adsorption simulation in RASPA. Hence it is imperative to block the inaccessible pockets to get accurate loading results for pure and quaternary gas mixture in RASPA.

4.2. Partition Function Results from JANAF and McQuarrie

In figure 4.2, the results of partition functions calculated using JANAF tables and equation from the Book by McQuarrie for NO_2, N_2O, O_2, N_2O_4 and NO are plotted vs temperature. In figure 4.2, the solid green line (N_2O_4_J) represents the partition function of N_2O_4 calculated using JANAF table, whereas the hollow green symbol (N_2O_4_MQ) represents the partition function of N_2O_4 calculated using equations from the book McQuarrie.

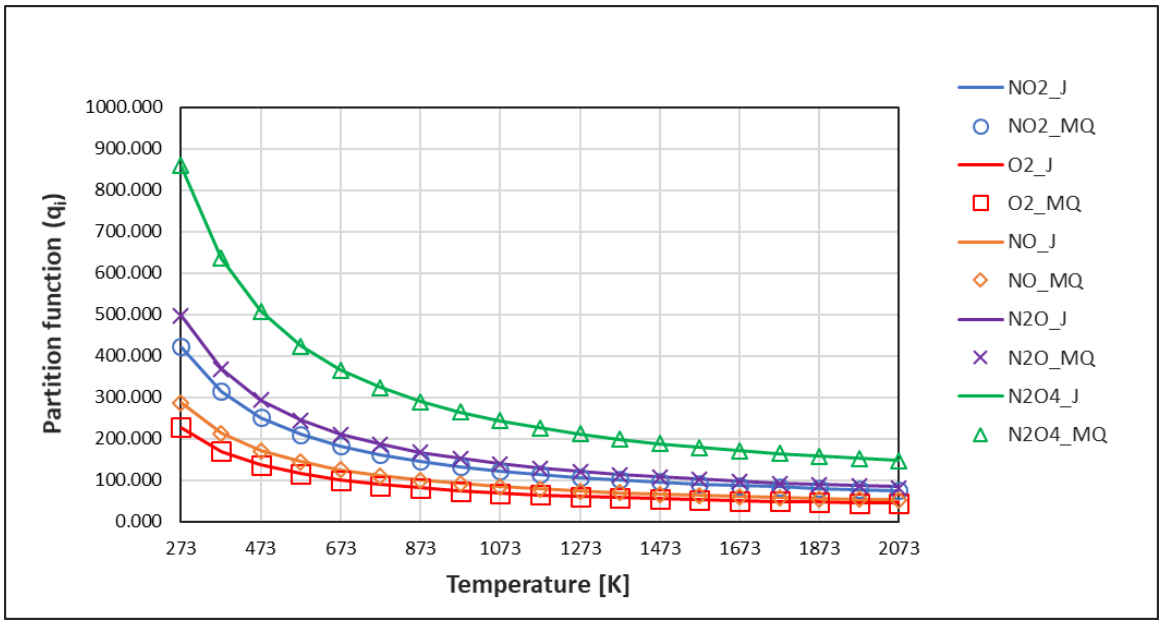

Figure 4.2: Partition function results calculated using equations from the book Donald McQuarrie and JANAF tables[17, 20], for NO_2, N_2O, O_2, N_2O_4 and NO. The solid lines represent partition function values calculated using equations from the book by Donald McQuarrie. The hollow symbols represent the partition function calculated using JANAF tables.

Similarly, the solid red line (O_2_J) represents the partition function of O_2 calculated using the JANAF table. In contrast, the hollow red symbol (O_2_MQ) represents the partition function of O_2 calculated using equations from the book McQuarrie. The solid blue line (NO_2_J)

in figure 4.2 represents the partition function of NO_2 calculated using the JANAF table. In contrast, the hollow blue symbol (NO_2_MQ) represents the partition function of NO_2 calculated using equations from the book McQuarrie. The solid purple line (N_2O_J) represents the partition function of N_2O calculated. In contrast, the table, whereas the hollow purple symbol (N_2O_MQ) represents the partition function of N_2O calculated using equations from the book McQuarrie and The solid orange line (NO_J) represents the partition function of NO calculated. In contrast, the table, whereas the hollow orange symbol (NO_MQ), represents the partition function of NO calculated using equations from the book McQuarrie. The values of the partition function for all the five components calculated using the JANAF table are in good agreement with the values calculated using equations from McQuarrie. These values of partition function are used as an input to (isobaric-isothermal) reaction ensemble. Partition function can also be obtained using quantum calculations in Gaussian09. Due to the lack of data available for quantum calculation and large deviation in results reported in previous work[22], hence the partition functions were not obtained using quantum calculations Gaussian09. For Reaction Monte Carlo simulations, JANAF values were used as an input because of good accuracy in reaction ensemble results, as reported in previous study[16, 22]. The partition values of NO_2, N_2O, O_2, N_2O_4 and NO obtained using JANAF tables and equations from the book McQuarrie and used as an input to reaction ensemble are tabulated in section A in tables A.1 and A.2.

4.3. Reaction Monte Carlo and Gibbs Minimization Results

In this section, The results from isobaric-isothermal reaction ensemble for equilibrium gas-phase reactions 3.3, 3.4, and 3.5 at 1 bar and 10 bar pressure and varying temperature from 273 K to 2073 K, computed using Brick are discussed. The NPT-RxMC results were validated using the Gibbs minimization technique at the same pressure, temperature, and composition as in NPT-RXMC.

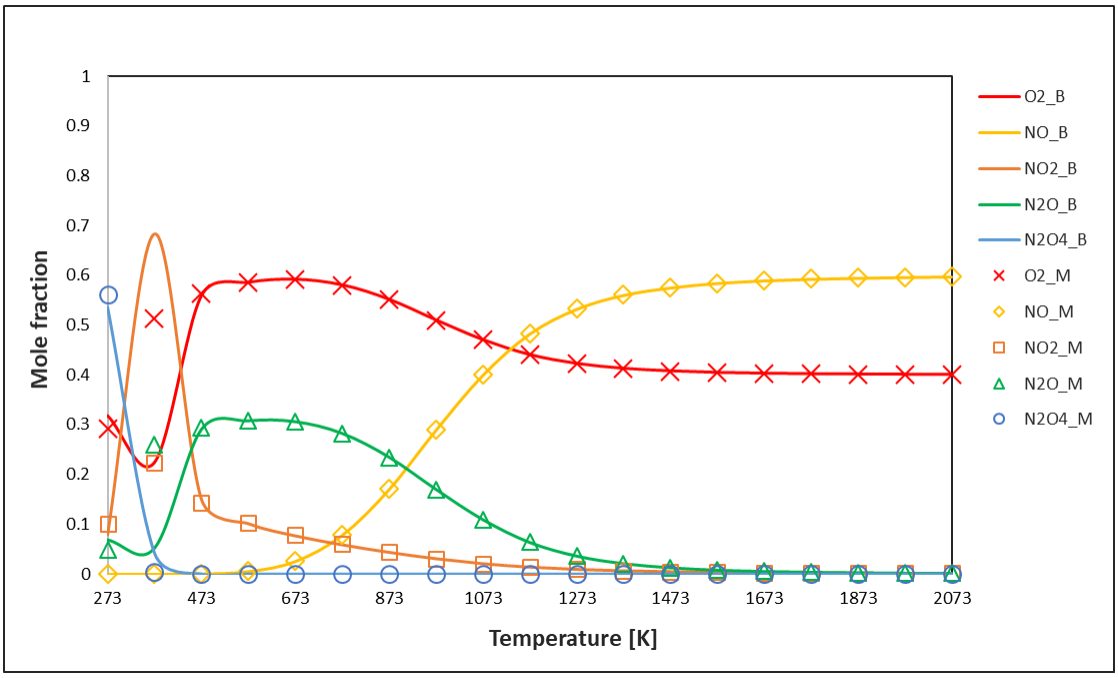

Figure 4.3: The Mole fractions results of NO_2, N_2O, O_2, N_2O_4, and NO at 1 bar pressure and (273 K-2073 K) temperature, computed using NPT-RXMC ensemble simulations in Brick and Gibbs minimization simulations from MATLAB. The solid lines represent mole fraction calculated using Brick, and the hollow symbols represent the mole fraction computed using Gibbs minimization in MATLAB.

Figure 4.3 represents mole fractions of NO_2, N_2O, O_2, N_2O_4 and NO at 1 bar pressure and (273 K-2073 K) temperature. The solid red line (O_2_B) in figure 4.3 represents the mole fraction of O_2 computed using Brick, whereas the red hollow symbol (O_2_M) represents the mole fraction of O_2 computed in MATLAB using Gibbs minimization. Similarly, the green, blue, yellow and orange solid lines in figure 4.3 represents the mole fraction of N_2O, N_2O_4, NO and NO_2 computed in Brick and the green, blue, yellow and orange hollow symbols in figure 4.3 represents the mole fraction of N_2O, N_2O_4, NO and NO_2 calculated in MATLAB. It can be observed from the figure 4.3 that the results from the NPT-RXMC ensemble simulations in Brick are in great agreement with the Gibbs minimization results from MATLAB simulations. In the case of NO_2, N_2O, and O_2, there are slight deviations in the results at low-temperature 373 K. Even after increasing the number of equilibration cycles from $1{\times}10^5$ to $3{\times}10^5$ in Brick simulation, there was no significant change in the results at 373 K. These variations can be due to the lower number of molecules in the simulation box or due to smaller cutoff radius as compared to the box size. Similar kinds of a problem were faced while working on the single reaction 3.3 NPT-reaction ensemble in Brick.

(Matito et al.), who studied the equilibrium reaction 3.3 using NPT-RXMC in RASPA and (Chao et al.), who performed the experimental study for the equilibrium reaction 3.3 at 1 atm - 5 atm pressure and 273 K-404 K temperature reported some similar results. NO_2 and N_2O_4 exits as monomer and dimer till 404 K. At higher temperatures, only the monomer NO_2 is present in the gas phase, as reported in the previous studies. At higher temperature N_2O_4 is converted to NO_2[4, 16]. (Matito et al.) reported the mole fraction of N_2O_4 to be 0.87 and NO_2 as 0.13 at 273 K and 1 atm pressure, which is almost equivalent to 1.013 bar. Chao et .al who performed experimental study also reported the mole fraction of N_2O_4 to be 0.875 and NO_2 as 0.125 at 273 K and 1 atm pressure[4, 16]. From this study, in the presence of three reactions 3.3, 3.4 and 3.5, the mole fraction of N_2O_4 and NO_2 at 1bar pressure and 273 K temperature was reported to be 0.53531 and 0.07872, this results are available in section C. Similarly, (Matito et al.) reported the mole fraction of N_2O_4 to be 0.051 and NO_2 as 0.949 at 375 K and 1 atm pressure and (Chao et al.) who performed experimental study reported the mole fraction of N_2O_4 to be 0.945 and NO_2 as 0.055 at 375 K and 1 atm pressure. From this study the mole fraction of N_2O_4 and NO_2 at 373 K and 1 bar pressure and in the presence of three reactions 3.3, 3.4 and 3.5 were reported to be 0.68239 and 0.04189. The good finding from the results in figure 4.3 is that the dimer mole fraction goes to zero at a temperature higher than 404 K, as reported in previous studies[4, 16]. Even in the case of NO, The mole fraction of NO is reported to be quite low at lower temperature and starts to increase as temperature rises above 773 K. Similar findings regarding the behavior of mole fractions of NO were reported in previous studies [8, 25]. The results for NO in figure 4.3, represent the similar behavior as mentioned about NO in the literature[8, 25]. It can be observed that in figure 4.3 the NO mole fraction starts increasing rapidly as temperature increases beyond 773 K. N_2O and NO_2 depict similar behavior, at a lower temperature, about 273 K, where the N_2O and NO_2 composition is quite low. Their composition increases with the increasing temperature. In the case of NO_2, the composition is quite high till 373 K and decreases as temperature goes on increasing[16]. Similarly, N_2O mole fraction increase from 473-673 K, and then it starts to decrease as temperature increases. At higher temperatures, most of the N_2O and NO_2 gas gets converted to O_2 and N_2, and as temperature increases beyond 773K, some of N_2O and NO_2 gas starts converting to NO and O_2[25]. At higher temperatures, more than 1073 K, the composition O_2 starts to decrease, and the composition of NO starts to increase in the system[25]. Similar results can be observed in figure 4.3. The results for the mole fraction of NO_2, N_2O, O_2, N_2O_4, and NO at 1 bar pressure and 273 K - 2073 K temperature from NPT-RXMC simulations in Brick and Gibbs minimization method in MATLAB can be found

in section C in table C.1 and C.2.

To comply with the operating conditions obtained from the company, the NPT-RXMC simulations in Brick and Gibbs minimization simulations in MATLAB were also performed at 10 bar pressure. The results of the simulations are shown in figure 4.4

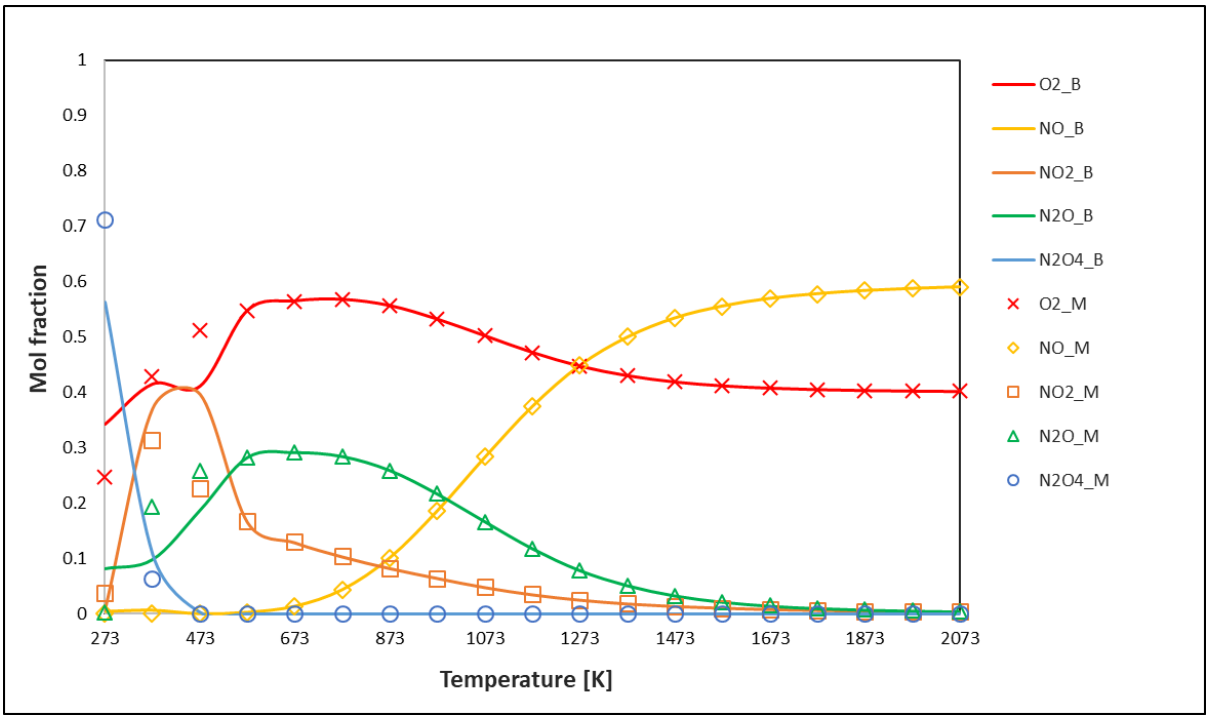

Figure 4.4: The Mole fractions results of NO_2, N_2O, O_2, N_2O_4, and NO at 10 bar pressure and (273 K-2073 K) temperature, computed using NPT-RXMC ensemble simulations in Brick and Gibbs minimization simulations from MATLAB. The solid lines represent mole fraction calculated using Brick, and the hollow symbols represent the mole fraction computed using Gibbs minimization in MATLAB.

It can be observed in figure 4.4 there are again small deviations in the results of NO_2, N_2O, O_2, N_2O_4 at 273 K, 373 K and 473 K. But it can be seen in the figure 4.4 that the results from Brick and MATLAB are in good agreement at a temperature above 473 K. If we compare the results from figure 4.3 at pressure 1 bar and 4.4 at pressure 10 bar, the difference in the values of mole fraction is quite less, and hence the comments made above regarding the behavior of mole fraction for NO_2, N_2O, O_2, N_2O_4, and NO at 1bar pressure and varying temperature ranging from 273-2073 K are applicable to the results displayed in figure 4.4 at 10 bar pressure. The mole fractions obtained from Brick at 10 bar pressure and 773 K temperature (operating conditions), were implemented in RXMC-GCMC simulations for the quaternary gas mixture (NO_2, N_2O, O_2, and NO) to obtain adsorption isotherms in RASPA. The results for the mole fraction of NO_2, N_2O, O_2, N_2O_4, and NO at 1 bar pressure and 273 K - 2073 K temperature from NPT-RXMC simulations in Brick and Gibbs minimization method in MATLAB can be found in section C in table C.3 and C.4.

4.4. GCMC Simulation Results for Pure Component Adsorption Isotherms

The pure component adsorption loading in mol/kg for NO_2, O_2, N_2O, and NO in MFI, MOR, TON, FAU, and FER zeolite at 773 K temperature and 1 bar - 15 bar pressure was obtained

through molecular simulation software RASPA. In this section, the adsorption isotherms for the pure components in MFI, followed by MOR, FAU, TON, and FER, are discussed and compared with the literature results. In figure 4.5 sub-figure (a) and sub-figure (b) represents pure NO_2, O_2, N_2O, and NO adsorption isotherms at 773 K and 1-15 bar temperature and pressure, in MFI and MOR. Similarly, figure 4.6 sub-figure (a) and sub-figure (b) represents pure NO_2, O_2, N_2O, and NO adsorption isotherms in FAU and TON at 773 K temperature and 1 bar - 15 bar pressure and figure 4.7 represents pure NO_2, O_2, N_2O, and NO adsorption isotherms in FER at the same temperature and pressure conditions.

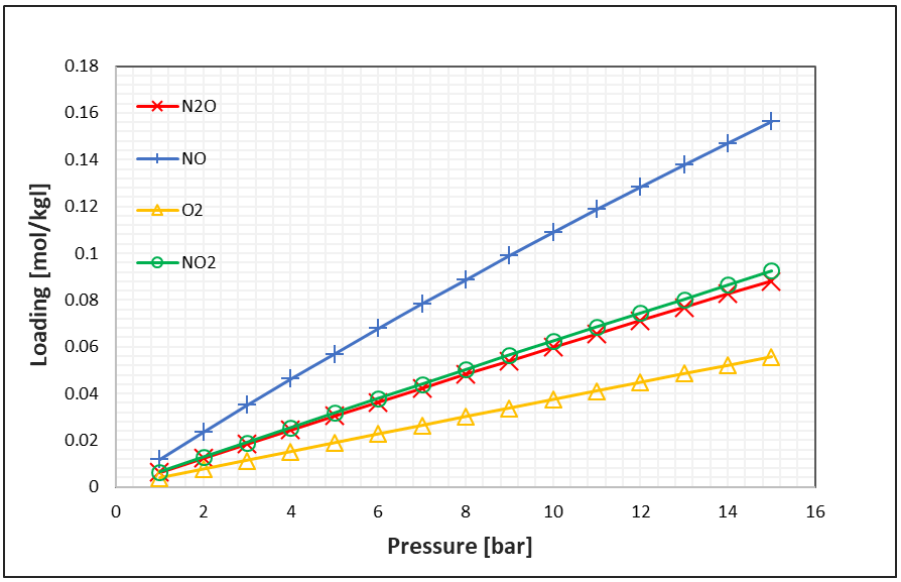

(a)

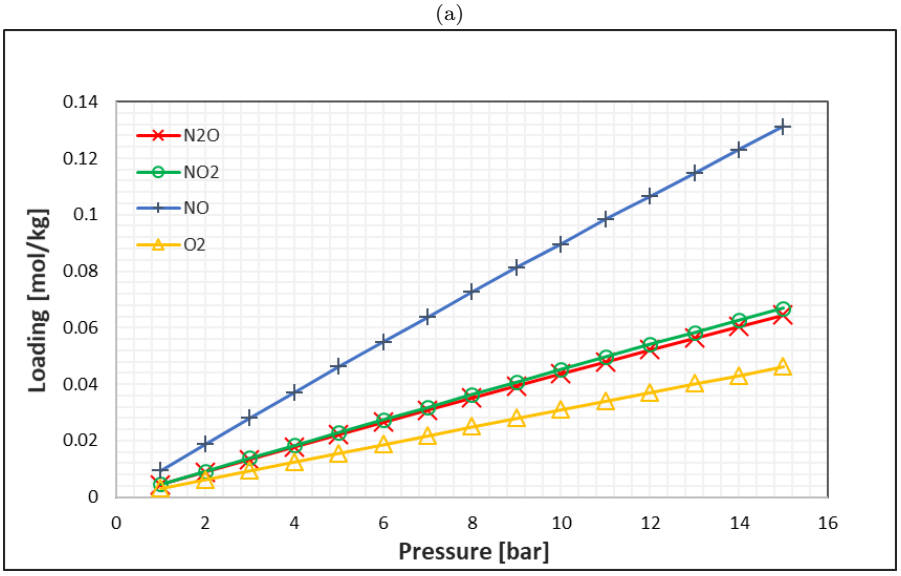

(b)

Figure 4.5: NO_2, O_2, N_2O, and NO adsorption isotherms in MFI and MOR at 773 K temperature and 1 bar - 15 bar pressure. Here, a solid red line with an empty red symbol represents loading in mol/kg for N_2O. The solid green line and empty green symbol represent loading for NO_2. The solid blue line with an empty blue symbol represents loading for NO, and the solid yellow line with an empty yellow symbol represents loading for O_2.

One can view from the figures 4.5, 4.6 and 4.7, NO has the highest loading in mol/kg in all the five zeolites, whereas O_2 has the lowest loading in all the five zeolites. It can be checked in

figures 4.5, 4.6 and 4.7, NO_2 and N_2O have similar loading behavior in MFI, MOR, TON, and FER. In the case of FAU, the adsorption of NO_2 and N_2O is quite identical. The loading of all the components in all frameworks starts at 1 bar and keeps on increasing till 15 bar. The saturation point for all four pure components in five different zeolites is far from the reach, as one can observe from figures 4.5, 4.6 and 4.7 the loading keeps on increasing with increasing pressure. NO has the highest loading in FAU, with the loading of 0.175 mol/kg at 15 bar pressure and 773 K temperature, followed by MFI, where the loading of NO is 0.15 mol/kg. In MOR, the loading of NO was 0.13 mol/kg, which is quite close to MFI loading, but in TON and FER, the loading of NO was very low, with 0.08 mol/kg in TON and lowest in FER, which was 0.068 mol/kg.

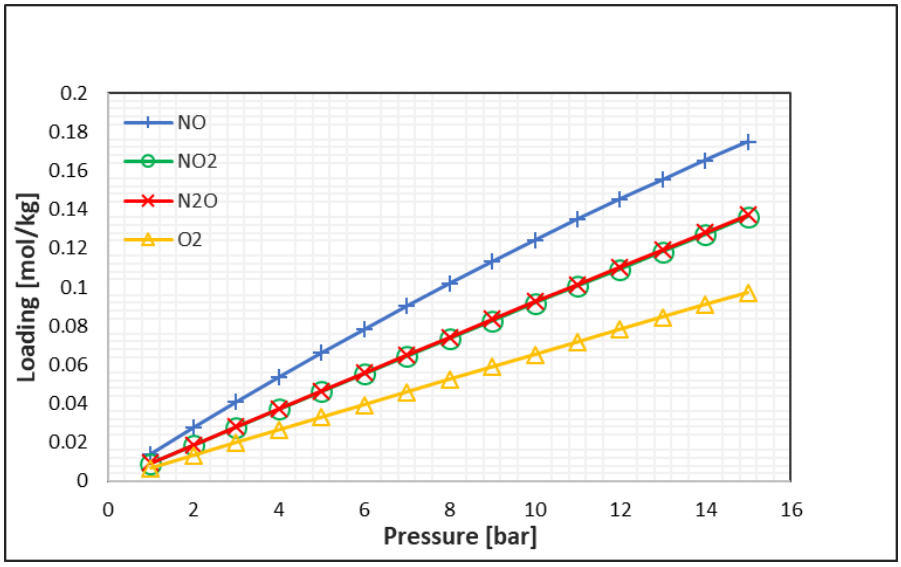

(a)

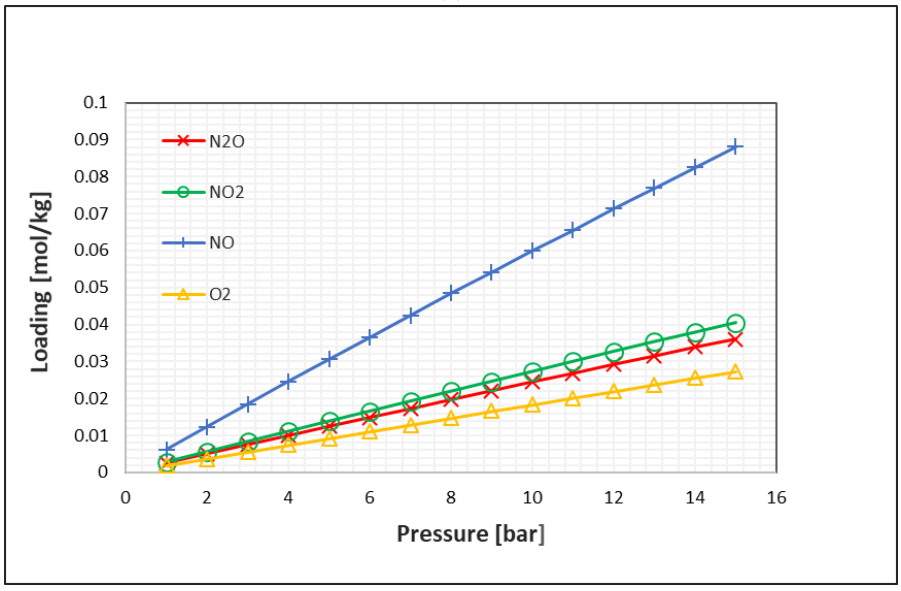

(b)

Figure 4.6: NO_2, O_2, N_2O, and NO adsorption isotherms in FAU and TON at 773 K temperature and 1 bar - 15 bar pressure. Here, a solid red line with an empty red symbol represents loading in mol/kg for N_2O. The solid green line and empty green symbol represent loading for NO_2. The solid blue line with an empty blue symbol represents loading for NO, and the solid yellow line with an empty yellow symbol represents loading for O_2.

The NO loading is highest in FAU, because of the availability of high pore volume with its specific volume of 0.332 cm^3/g[16]. This is followed by MFI whose specific volume is 0.164 cm^3/g, MOR with specific volume 0.15 cm^3/g, TON with specific volume 0.091 cm^3/g and FER with specific volume 0.066 cm^3/g[16]. Similarly, NO_2 and N_2O showed the highest and similar adsorption loading of O.137 and 0.136 mol/kg in FAU at 15 bar and 773 K, whereas NO_2 and N_2O loading in MFI is 0.092 and 0.088 mol/kg at same operating conditions. In the case of TON, whose framework topology is quite similar to MOR but has no side pockets and low pore volume, the loading in TON for NO_2 and N_2O was 0.04 and 0.036 mol/kg at 15 bar pressure and 773 K temperature.

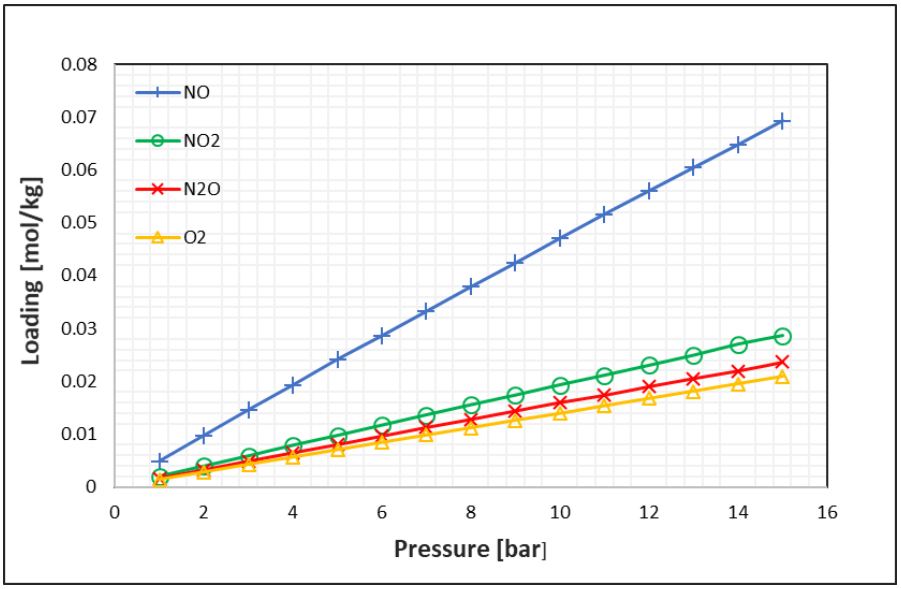

Figure 4.7: NO_2, O_2, N_2O, and NO adsorption isotherms in FER at 773 K temperature and 1 bar - 15 bar pressure. Here, a solid red line with an empty red symbol represents loading in mol/kg for N_2O. The solid green line and empty green symbol represent loading for NO_2. The solid blue line with an empty blue symbol represents loading for NO, and the solid yellow line with an empty yellow symbol represents loading for O_2.

For FER whose pore volume is lowest amongst all the framework, the loading for NO_2 and N_2O were reported as low as around 0.028, and 0.023 mol/kg at the same operating conditions. O_2, which showed the weakest adsorption behavior of all the five components, showed similar adsorption loading behavior as in NO. In NO, FAU showed 0.097 mol/kg loading, as in MFI NO loading was 0.055 mol/kg, followed by 0.046 mol/kg in MOR, 0.027 mol/kg in TON, and 0.02 mol/kg in FER at 15 bar pressure and 773 K temperature. In case of NO, NO_2 and N_2O and O_2 following pattern of loading was observed (FAU>MFI>MOR>TON>FER). I compared the results from this work with the results from previous work for the pure component loading. (Weizhen et al.) studied pure NO_2, NO, and O_2 loading in FAU and MFI at 313 K and 0 kPa - 100 kPa pressure. (Weizhen et al.) reported the loading of NO in FAU to be 0.094 mol/kg at 100 kPa pressure, which is equal to 1 bar and 313 K[29] whereas the loading of NO is reported to be 0.182 mol/kg at 1 bar and 313K in MFI[29]. This study reported the loading of NO at 1 bar pressure and 773 K temperature to be 0.013 mol/kg in FAU and 0.012 mol/kg in MFI. From the comparison of the results, one can see that the higher the temperature, the higher is the effect on the loading of NO in FAU and MFI. At low temperature, the loading of NO was quite high in MFI compared to FAU as per the results from (Weizhen et al.). In the case of NO_2, (Weizhen et al.) reported the loading to be 0.156 mol/kg in FAU at 1 bar pressure and 313 K, whereas they also reported the loading of NO_2 to be 0.409 at 1 bar 313 K in MFI[29]. (Matito et al.) who studied the adsorption of pure NO_2 and N_2O_4 in MFI, FAU, FER, TON,

and FER also reported the loading of NO_2 at 1 bar and 10 bar pressure at 298 K temperature. (Matito et al.) reported NO_2 loading to be 0.87 mol/kg in MFI and 0.34 mol/kg in FAU at 1 bar pressure and 298 K temperature[16]. From this study, the loading of NO_2 in MFI was 0.006 mol/kg, and 0.009 mol/kg in FAU at 1 bar and 773 K. Whereas, (Matito et al.) reported the loading of NO_2 in MFI to be 2.648 mol/kg and 3.4 mol/kg in FAU, at 10 bar pressure and 298 K temperature. In this study, the reported loading of NO_2 in MFI and FAU at 10 bar pressure and 773 K temperature was 0.06 mol/kg and 0.09 mol/kg. From the results at 10 bar pressure, one can observe that the adsorption of NO_2 is higher in FAU at higher pressure as compared to MFI, but it is another way around at low pressure and low temperature. This study reports the NO_2 loading to be highest in FAU, followed by MFI, MOR, TON, and FER for 1-10 bar pressure and 773 K temperature. Similar behavior of NO_2 loading was reported by (Matito et al.) in all the zeolites, which they studied at 10 bar pressure and room temperature[16]. (Weizhen et al.) reported the loading for O_2 to be 0.055 mol/kg in FAU and 0.074 mol/kg in MFI at 313 K temperature and 1 bar pressure[29]. In this study, the obtained O_2 loading was 0.006 mol/kg in FAU and 0.003 mol/kg in MFI at 1 bar and 773K. For O_2, one can also observe that at high temperature and low pressure, the adsorption of O_2 is quite low as compared to low temperature and low pressure. O_2 is adsorbed higher in MFI than in FAU at low pressure and low-temperature conditions, But at high temperature and pressure, 773K and 10 bar, FAU has higher loading as compared to MFI. This was reported by (Matito et al.) in case of NO_2 and N_2O_4[16]. Unfortunately, for N_2O, the loading data for similar zeolite is not available, But the adsorption behavior of N_2O, as reported here, is quite similar to NO_2. The pure component adsorption data for NO_2, O_2, N_2O, and NO obtained from this simulation in RASPA was further used to validate the quaternary gas mixture simulation data obtained from RASPA using ideal adsorbed solution theory in python.

4.5. Quaternary Gas Mixture Adsorption Isotherms from RXMC- GCMC Simulations

The results of the quaternary gas mixture isotherms of NO_2, O_2, N_2O, and NO in MFI, MOR, TON, FAU, and FER at 1 bar - 15 bar pressure and 773 K temperature are shown here. The results were obtained after performing a quaternary gas mixture reactive Grand Canonical Monte Carlo simulations in RASPA. For RXMC-GCMC quaternary gas mixture simulation in RASPA, the mole fraction of all the components for equilibrium bulk phase composition obtained from the isobaric-isothermal reaction ensemble has to be specified. The mole fractions for NO_2, O_2, N_2O, and NO at 773 K and 10 bar pressures is mentioned in section 4.3 and is shown in figure 4.4. These results were implemented during the RXMC - GCMC simulations. The mole fractions of NO_2, O_2, N_2O, and NO at 773 K and 10 bar pressure computed using isobaric-isothermal reaction ensemble in Brick and Gibbs minimization in MATLAB are tabulated in table 4.1.

Component	Mole fraction (Brick)	Mole fraction (MATLAB)
O_2	0.56826	0.56735
N_2O	0.28461	0.28395
NO_2	0.10322	0.10471
NO	0.04391	0.04398

Table 4.1: Mole fraction of NO_2, O_2, N_2O, and NO at 773 K and 10 bar pressure computed using isobaric-isothermal reaction ensemble in brick and Gibbs minimization in MATLAB.

The Mole fraction results from Brick's reaction ensemble simulations were implemented in

RXMC - GCMC quaternary gas mixture simulations in RASPA. One can also notice that N_2O_4 was not included during the RXMC - GCMC simulations as the mole fraction of N_2O_4 is almost zero after 404 K[16]. This can be found in figure 4.4 and the data can be found in section C in table C.3 and C.4. In figure 4.8 sub-figure (a) and sub-figure (b) represents the adsorption isotherms for the quaternary mixture of NO_2, O_2, N_2O, and NO at 773 K temperature and 1 bar - 15 bar pressure in MFI and MOR. Similarly figure 4.8 sub-figure (a) and sub-figure (b) represents the adsorption isotherms for the quaternary mixture of NO_2, O_2, N_2O, and NO at 773 K temperature and 1 bar - 15 bar pressure in FAU and TON. Figure 4.10 represents adsorption isotherms for a quaternary mixture of NO_2, O_2, N_2O, and NO at the same operating conditions in FER.

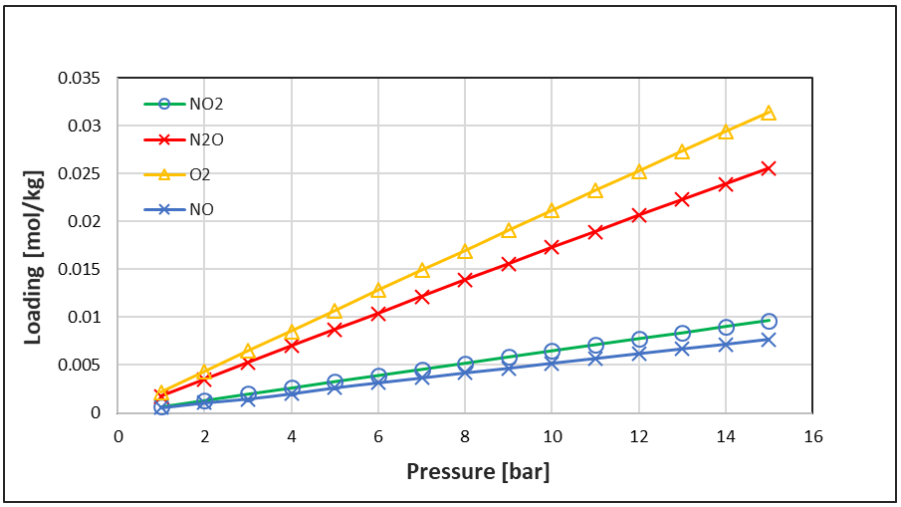

(a)

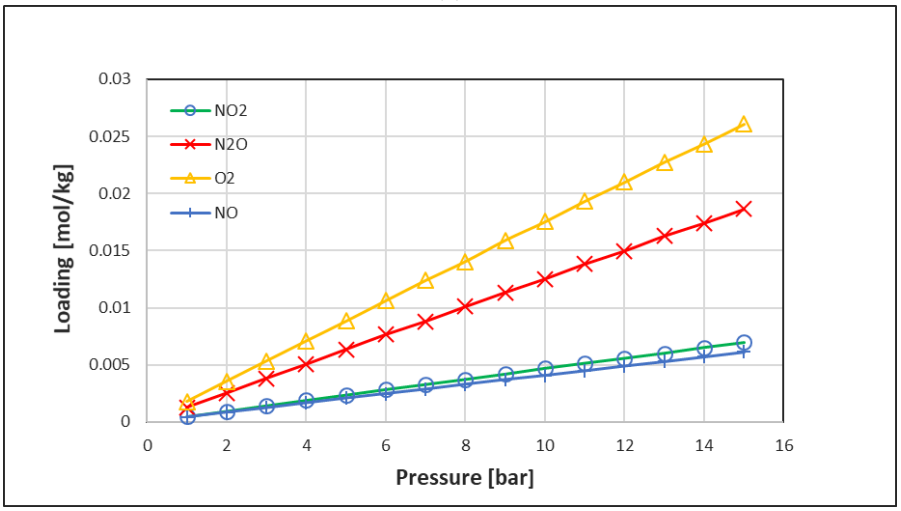

(b)

Figure 4.8: Quaternary mixture adsorption isotherms in MFI and MOR at 773 K temperature and 1 bar - 15 bar pressure. Here, a solid red line with an empty red symbol represents loading in mol/kg for N_2O. The solid green line and empty green symbol represent loading for NO_2. The solid blue line with an empty blue symbol represents loading for NO, and the solid yellow line with an empty yellow symbol represents loading for O_2.

These results were further verified using the ideal adsorbed solution theory. From table 4.1, it can be observed that the mole fraction of O_2 from RXMC simulations was highest at 773 K temperature and 10 bar pressure. The mole fraction of NO was reported to be lowest around 0.04391. This is because NO composition starts increasing at a higher temperature (see section

4.3). Similarly, NO_2 and N_2O mole fraction at 773 K and 10 bar were 0.10322 and 0.28461. Depending on the mole fraction results for various components at 773 K and 10 bar it can be observed in figure 4.8 sub-figure (a) and sub-figure (b), figure 4.8 sub-figure (a) and sub-figure (b), and figure 4.10, O_2 has the highest loading in mol/kg in all the zeolites, whereas NO has the lowest loading in all the zeolites. Nitrous oxide (N_2O) loading was also higher than the loading of Nitrogen oxide NO_2 in all the zeolite, but N_2O loading was lower than O_2 in all the frameworks. Loading of all the components in all the zeolites commenced at 1 bar, but there was no saturation observed as the loading continued increasing with increasing pressure. In figure 4.8 subfigure (a) the loading of O_2 in MFI at 15 bar pressure, and 773 K temperature was reported to be 0.031 mol/kg. N_2O loading in MFI at the same operating conditions was reported as 0.025 mol/kg. Whereas NO_2 and NO loading in MFI at 15 bar and 773 K pressure and temperatures was around 0.009 mol/kg and 0.007 mol/kg.

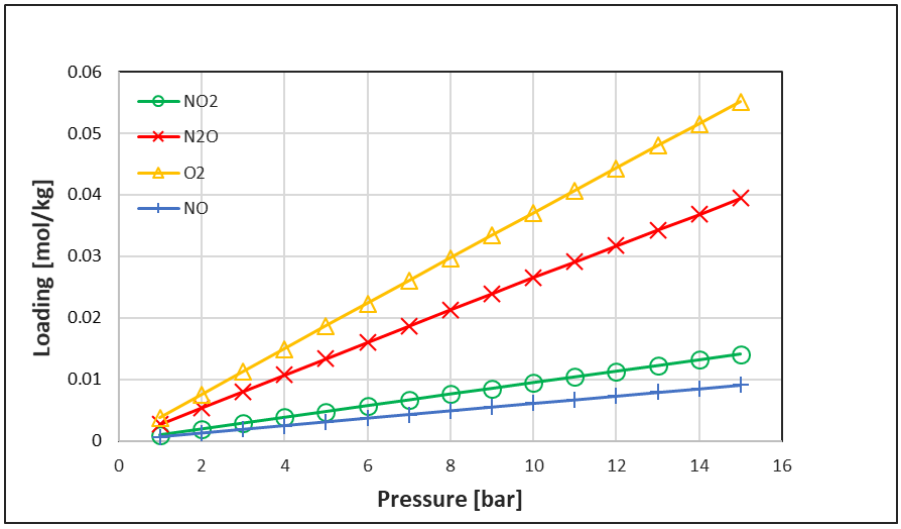

(a)

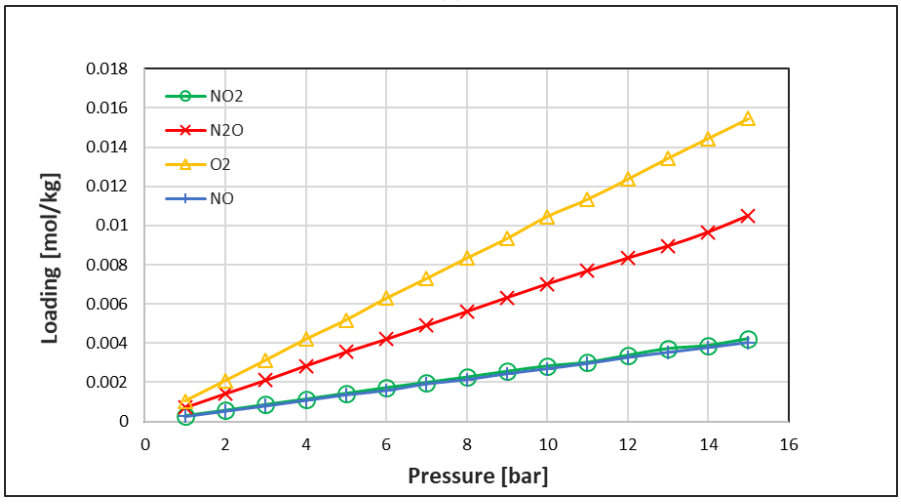

(b)

Figure 4.9: Quaternary mixture adsorption isotherms in FAU and TON at 773 K temperature and 1 bar - 15 bar pressure. Here, a solid red line with an empty red symbol represents loading in mol/kg for N_2O. The solid green line and empty green symbol represent loading for NO_2. The solid blue line with an empty blue symbol represents loading for NO, and the solid yellow line with an empty yellow symbol represents loading for O_2.

In MOR, as represented in figure 4.8 sub-figure (b) O_2 loading was 0.026 mol/kg at 773 K and 15 bar. N_2O loading was reported as 0.018 mol/kg at the same operating conditions. NO, and

NO_2 loading was 0.07 mol/kg and 0.061 mol/kg at 15 bar pressure and 773 K temperature. It can be observed that the results from MOR are within reach of MFI. This is because MFI and MOR have quite similar structural pore volume, but MFI has a higher specific volume than MOR, so the loading is higher in MFI. In the case of TON and FER as represented in figure 4.9 subfigure (b) and figure 4.10 the loading of NO_2 and NO shows similar behavior. But the loading of NO and NO_2 is higher in TON with 0.0042 mol/kg of NO_2 and 0.0040 mol/kg of NO at 773 K and 15 bar as compared to the loading of NO_2 which is 0.0030 mol/kg and NO O.0029 mol/kg in FER at same operating conditions. The loading for N_2O and O_2 in TON was reported to be 0.01 mol/kg and 0.015 mol/kg at 773 K and 15 bar. This was a bit lower as compared to MOR, as MOR and TON have similar topologies, but TON has no side pockets.

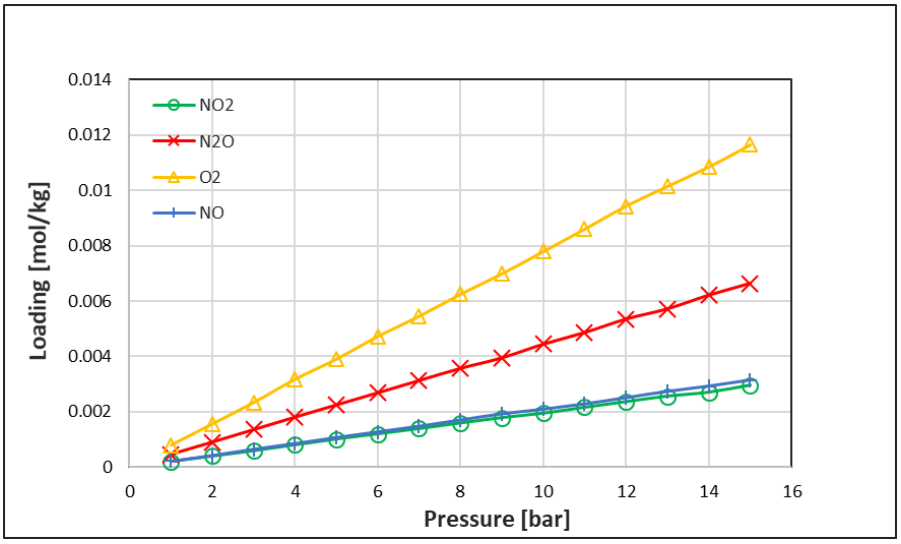

Figure 4.10: Quaternary mixture adsorption isotherms in FER at 773 K temperature and 1-15 bar pressure. Here, a solid red line with an empty red symbol represents loading in mol/kg for N_2O. The solid green line and empty green symbol represent loading for NO_2. The solid blue line with an empty blue symbol represents loading for NO, and the solid yellow line with an empty yellow symbol represents loading for O_2.

In the case of FER, the Loading of O_2 and N_2O was 0.01 mol/kg and 0.006 mol/kg, at the same operating conditions. The last zeolite is FAU, which exhibited the highest loading of all the components at 773 K and 15 bar pressure. The loading of O_2 in FAU was 0.05 mol/kg were as for N_2O; it was 0.039 mol/kg at the same conditions. NO_2 loading was reported as 0.014 mol/kg in FAU, and NO loading in FAU was 0.009 mol/kg. FAU exhibit hight loading because of more number of pores and side pockets available in the framework and high specific volume. These results of quaternary mixture adsorption isotherms in MFI, MOR, FAU, FER, and TON from RXMC-GCMC simulations in RASPA had to be verified and hence ideal adsorbed solution theory was implemented to validate this results, which is discussed in the next part.

4.6. Validation of RXMC-GCMC Results Using Ideal Adsorbed Solution Theory

In this section, the results from RXMC-GCMC simulations in RASPA for the quaternary gas mixture, as discussed in section 4.5, are validated using the ideal adsorbed solution theory in python using the package pyiast. The validation of the results discussed in section 4.5 is achieved by comparing the results from section 4.5 with the results predicted by IAST. Figure 4.11, sub-figure (a) and sub-figure (b), whereas figure 4.6, sub-figure (a) and (b), represents the plots for validation of adsorption isotherms for the quaternary mixture of NO_2, O_2, N_2O, and NO obtained from RXMC-GCMC simulations in RASPA and the predicted isotherms from

IAST in MFI, MOR, FAU and TON at 773K temperature and 1-15 bar pressure. The y-axis of the figure 4.11, sub-figure (a) and (b), and figure 4.12, sub-figure (a) and (b), represents the loading in mol/kg. Whereas the x-axis represents partial pressure of O_2 in bar. Similarly figure 4.13 represents a plot for validation of adsorption isotherms for the quaternary mixture of NO_2, O_2, N_2O, and NO obtained from RXMC-GCMC simulations in RASPA and the predicted isotherms from IAST in FER. From the figure 4.8 sub-figure (a) and (b), and figure 4.9, subfigure (a) and (b), and also figure 4.10, one can observe the IAST predicted results for the quaternary mixture are in good agreement with the results obtained from RXMC-GCMC simulations in RASPA for all the five frameworks.

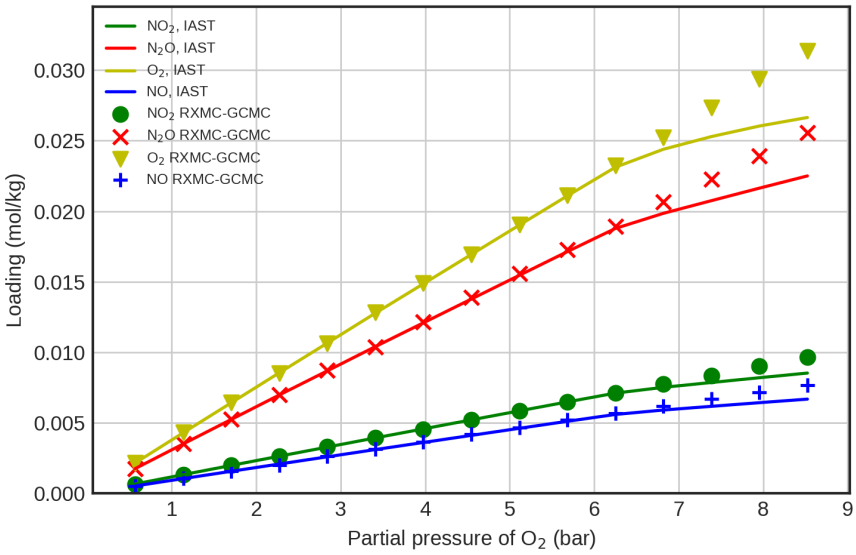

(a)

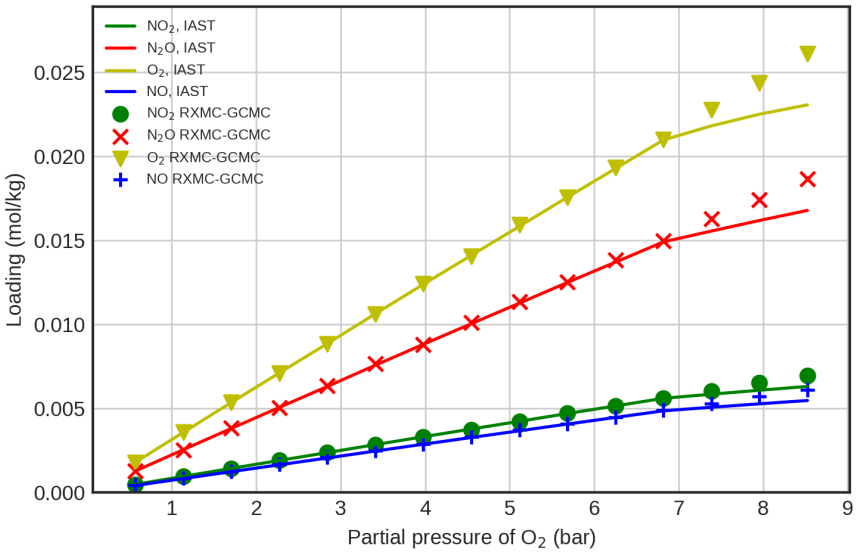

(b)

Figure 4.11: IAST validation of quaternary mixture adsorption isotherms of NO_2, O_2, N_2O, and NO in MFI and MOR at 773 K and 1 bar - 15 bar pressure. Here, solid yellow, red, green, and blue lines represent loading prediction by IAST in mol/kg for O_2, N_2O, NO_2, and NO in MFI and MOR predicted by IAST. The solid yellow, red, green, and blue symbols represent quaternary mixture loading of O_2, N_2O, NO_2, and NO in MFI and MOR obtained from RXMC-GCMC simulations in RASPA.

In the figure 4.11, sub-figure (a) NO_2 and NO adsorption isotherms from RXMC-GCMC simulations are in good accord with the IAST prediction for MFI. Still, in case of O_2 and N_2O, the prediction and RXMC - GCMC results match quite well till seven-bar partial pressure, but there is quite some deviation at higher pressure between prediction and simulation results.

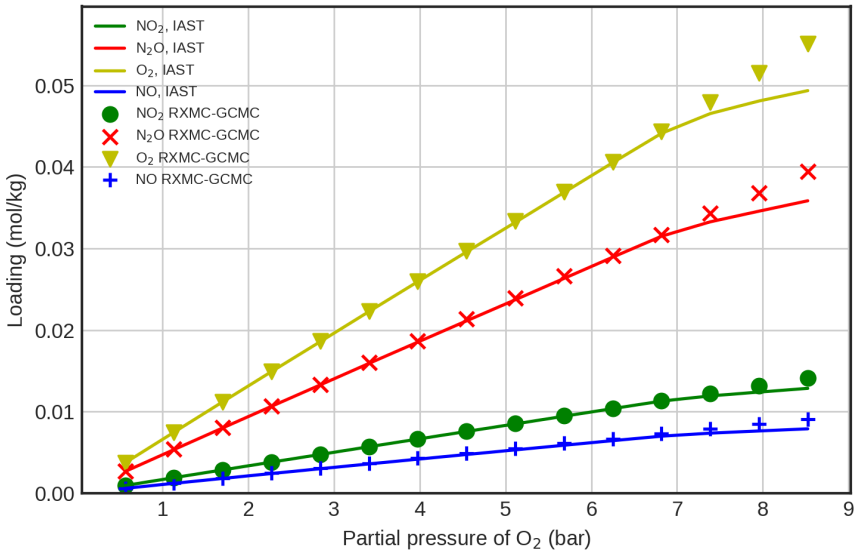

(a)

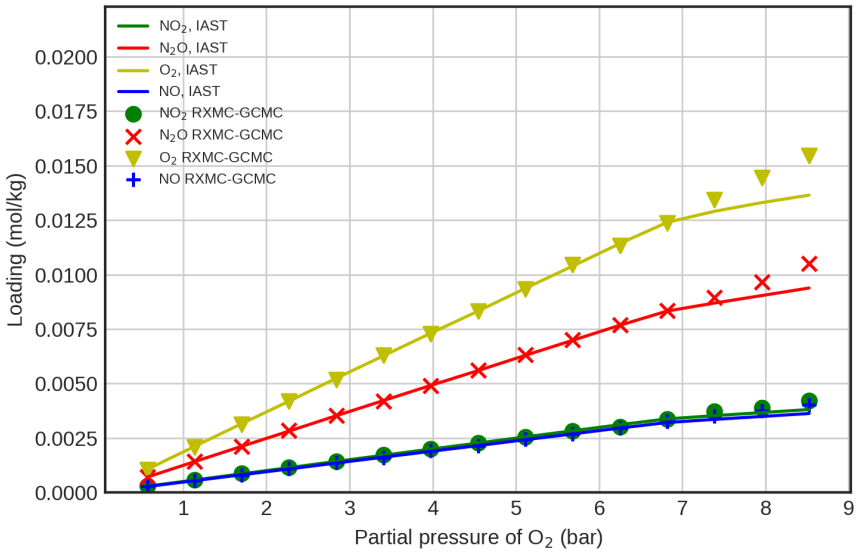

(b)

Figure 4.12: IAST validation of quaternary mixture adsorption isotherms of O_2, N_2O, NO_2, and NO in FAU and TON at 773 K and 1-15 bar pressure. Here, solid yellow, red, green, and blue lines represent loading prediction by IAST in mol/kg for O_2, N_2O, NO_2, and NO in FAU and TON predicted by IAST. The solid yellow, red, green, and blue symbols represent quaternary mixture loading of O_2, N_2O, NO_2, and NO in FAU and TON obtained from RXMC - GCMC simulations in RASPA.

similar behaviour is seen in figure 4.11, sub-figure (b) for MOR. In this case, NO_2, O_2, and NO predicted isotherms, and the RXMC-GCMC isotherms exhibit similar behavior as in MFI. But there is a slight improvement in the case of N_2O predicted and obtained isotherm. For

N_2O in MFI, the IAST prediction results and the RXMC-GCMC simulation results are very close to each other even at the higher partial pressure of O_2.

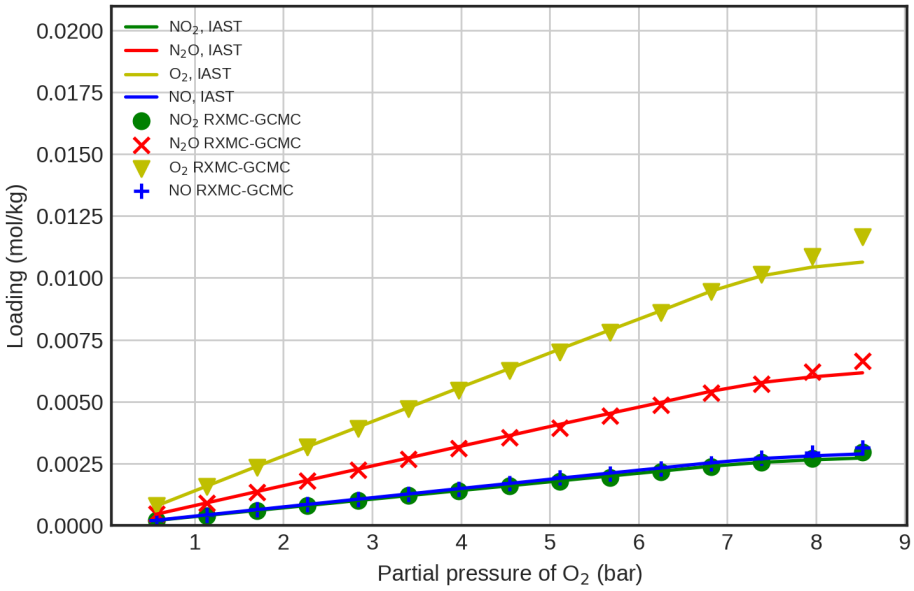

Figure 4.13: IAST validation of quaternary mixture adsorption isotherms of O_2, N_2O, NO_2, and NO in FER at 773 K and 1 bar - 15 bar pressure. Here, solid yellow, red, green, and blue lines represent loading prediction by IAST in mol/kg for O_2, N_2O, NO_2, and NO in FER predicted by IAST. The solid yellow, red, green, and blue symbols represent quaternary mixture loading of O_2, N_2O, NO_2, and NO in FER obtained from RXMC-GCMC simulations in RASPA

FAU and TON's, IAST prediction of isotherms for all the components, and RXMC-GCMC results showed a quite good agreement at a higher partial pressure of O_2 as shown in figure 4.12, sub-figure (a) and (b). The IAST prediction results for FAU and TON are quite good as compared to MOR and MFI. FER framework as shown in figure 4.13, showed a great agreement between IAST predicted isotherms and the isotherms from RXMC-GCMC simulations in RASPA as compared to MFI, MOR, FAU, and TON at similar operating conditions and for all the four components.

5

Conclusions and further research

In this work, molecular simulations were implemented to understand the behavior of the bulk phase equilibrium reactions at given operating conditions to reduce the emission of nitrogen oxides (NO_x) from the tail gas of nitric acid (HNO_3) production facility using porous materials like zeolites. The first step was to find the possible equilibrium reactions that carry the NO_x components like NO, N_2O, N_2O_4, and NO_2. The reaction that harbored these components were taken from the literature. The next step was to select the best possible frameworks, force fields, and charges for all the components and framework atoms involved in the simulations. This step was successfully completed by choosing the five zeolites, FAU, FER, MFI, MOR, and TON that were previously studied for some of the NO_x components mentioned here[16]. The partial charges and force-fields for all framework and component atoms implemented in this study were taken from the literature that showed good results from their study[10, 16, 29]. In the next step, it was essential to calculate partition functions for all the components involved in the reactions as the partition functions are the input to the reaction ensemble. The partition functions for all the components were successfully calculated and validated (see section A).

In the next step, The bulk phase isobaric-isothermal reaction ensemble simulations were successfully carried out in the Brick simulation package to determine the composition of all the NO_x components for varying temperature (273 K to 2073 K) and pressure at 1 bar and 10 bar. The mole fraction results form NPT-RXMC simulation were then validated using Gibbs minimization simulations in MATLAB. The results can be viewed in section 4.3 and section C. In the next step, pure component adsorption isotherms were obtained in all five zeolites using GCMC simulations in RASPA. Before this step was carried out, it was important to identify the inaccessible pockets in FAU and FER zeolites and block these pockets to avoid discrepancies in the adsorption results. The blocking process was successfully carried out in Zeo++ software. The results of blocking the pockets can be viewed in section 4.1. In the case of pure component, NO was the highest adsorbed component in all the five frameworks at 773 K temperature and 1-15 bar pressure, with FAU showing the highest loading of NO followed by MFI, MOR, TON, and lowest in FER. N_2O was the second-highest adsorbed component in all the five frameworks, followed by NO_2 and O_2. The adsorption behavior of N_2O, NO_2 and O_2 was similar to NO in all the five frameworks. FAU showed the best performance in adsorption of all the NO_x components because of a high specific volume and more pockets. This was followed by MFI, MOR, TON, and FER, which has the lowest volume and fewer pores. The results from the pure component adsorption were further successfully implemented for the validation of RXMC-GCMC quaternary gas mixture adsorption. The second last step in this study was

implementing the reactive Grand Canonical Monte Carlo method to study the adsorption of the quaternary mixture of NO, N_2O, O_2 and NO_2 at 773 K temperature and 1 bar - 15 bar pressure. The dimer Dinitrogen tetroxide was not considered because the composition of N_2O_4 at 773 K is zero. Only the monomer Nitrogen dioxide NO_2 exists at a temperature above 404 K. The composition of NO, N_2O, O_2 and NO_2 at 773 K and 10 bar pressure from bulk phase NPT-RXMC see section 4.3 was successfully implemented in RXMC-GCMC simulations for the quaternary gas mixture adsorption in RASPA. For this simulation, the mole fraction of O_2 was highest, followed by N_2O, NO_2, and NO. Hence NO was the lowest adsorbed component in all the five zeolites from RXMC-GCMC quaternary mixture simulations. Whereas O_2 was the highest adsorbed component followed by N_2O, NO_2 in all the five frameworks. The adsorption performance of all the five zeolites from RXMC-GCMC quaternary mixture simulations was similar to GCMC pure component simulations with FAU showing the highest loading followed by MFI, MOR, TON, and FER. The last step was to validate the RXMC-GCMC quaternary mixture simulations results from RASPA using the Ideal Adsorbed Solution Theory (IAST). The results from the RXMC-GCMC quaternary mixture simulations were validated, and the results are in good agreement with the IAST prediction of isotherms.

NO is the most important component in the HNO_3 production[21]. Whereas N_2O, whose composition is highest amongst the NO_x components at 773 K and 10 bar pressure, has to be adsorbed or separated from the tail gas as it has huge impacts on Ozone layer in the troposphere and on the health and environment[21]. From this study, it can be verified from section 4.5 N_2O is quite well adsorbed in all the zeolites and especially in FAU. The loading N_2O in FAU can still be improved, as there was no saturation obtained till 15 bar pressure. It might be possible to increase the loading of N_2O in FAU by increasing the pressure till the saturation point for adsorption of N_2O is reached in FAU. Another way is to adsorb more NO in FAU, as NO showed the highest adsorption in case of pure component loading in FAU (see section 4.4). If NO can be captured and reused in HNO_3 production process, doing so can increase the yield of HNO_3, and this has been reported in previous studies[21]. This can be achieved by performing RXMC-GCMC quaternary mixture simulations at higher temperature and pressure in the various zeolite. NO has its highest composition at a higher temperature above 2000 K, see section 4.3. The two benefits form this suggestion are, one at a higher temperature and pressure more NO can be adsorbed in zeolites, and the adsorbed NO can be reused for HNO_3 production, which in turn increases the yield of HNO_3. And the second solution is, at higher temperatures N_2O and NO_2 are mostly converted to NO and O_2 as their composition is almost negligible at a temperature above 1500 K see section 4.3. In this way, the emissions from N_2O and NO_2 can be reduced. The last thing is to perform an experimental study for adsorption of all the NO_x components in at least one of the five zeolites understudy or with some different zeolites to validate the simulation results.

Appendix-A

In this section, I will discuss the Partition functions calculated using the equations from the Book by Donald McQuarrie. Here I will demonstrate an example of partition function calculated for polyatomic non-linear molecule NO_2.
The ideal gas partition function of a molecule is given by equation A.1

$$q(T,V) = q_t(T,V) \times q_r(T) \times q_v(T) \times q_{el}(T) \tag{A.1}$$

where q_t(T,V), q_r(T), q_v(T) and q_{el}(T) are translation, rotation, vibration and electronic partition functions. The polyatomic partition function for non-linear NO_2 molecule is given by equation A.2

$$q(V,T) = \frac{V}{\Lambda^3}.\frac{\pi^{0.5}}{\sigma}\left(\frac{T^3}{\Theta_{rot,a},\Theta_{rot,b},\Theta_{rot,c}}\right) \times \prod_{j=1}^{(3n-6)} \frac{1}{1-exp[-\Theta_{vib,j}/T]}.g_{e1}e^{D_0/k_bT} \tag{A.2}$$

Here, the values of $(\Theta_{rot,a},\Theta_{rot,b},\Theta_{rot,c})$ the rotational temperatures, vibrational temperatures $(\Theta_{vib,j})$ and the atomization energy D_o for NO_2 molecule, are taken from book by Donald McQuarrie chapter 18 table 18.4 [17, 20]. For simplicity lets consider reference partition function q°(V,T). where;

$$q^{\circ}(V,T) = \frac{V}{\Lambda^3}.\frac{\pi^{0.5}}{\sigma}\left(\frac{T^3}{\Theta_{rot,a},\Theta_{rot,b},\Theta_{rot,c}}\right) \times \prod_{j=1}^{(3n-6)} \frac{1}{1-exp[-\Theta_{vib,j}/T]}.g_{e1} \tag{A.3}$$

Hence equation A.2 can be also written

$$q(V,T) = q^{\circ}(V,T).e^{D_0/k_bT} \tag{A.4}$$

The value of the symmetry number σ in the equation A.2 is taken from the table 2.1 from section 2.1.3. After plugging in all the values, and performing the conversions using equation 3.7 as mentioned in section 3.2.4 the partition function of polyatomic non-linear molecule NO_2 at 273 K temperature is found to be,

q(V,T)_NO_2= 422.70, This value of the partition can be used as an input to Brick simulation software.

Here an example of Partition function for non-linear molecule NO_2 is calculated using JANAF tables.
The ideal gas standard chemical potential is given by equation A.5

$$\mu^{\circ}(T) = -RTln\left[\left(\frac{q(V,T)}{V}\right)\frac{k_bT}{P^{\circ}}\right] \tag{A.5}$$

Here P° is the standard reference pressure, which is 1.0133×10^5 pa or almost equivalent to 1 bar.

$$\mu^{\circ}(T) - E^{\circ}(0K) = -RTln\left[\left(\frac{q^{\circ}(V,T)}{V}\right)\frac{k_bT}{P^{\circ}}\right] \tag{A.6}$$

And for a molecule at T=0 K the standard molar enthalpy $H^{\circ}(0\ \mathrm{K}) = E^{\circ} = -D_0$ (atomization energy).

For a pure component $\mu^{\circ} = G^{\circ}$ and hence, $(\mu^{\circ}(\mathrm{T}) - E_0^{\circ})$ is represented as $(G^{\circ}(T)\text{-}H_0^{\circ})$ in the JANAF table as shown in fig A.1.

Nitrogen Oxide (NO_2) $N_1O_2(g)$

Enthalpy Reference Temperature = T_r = 298.15 K Standard State Pressure = p° = 0.1 MPa

	J·K^{-1} mol^{-1}			kJ·mol^{-1}			
T/K	C_p°	S°	$-[G^{\circ}-H^{\circ}(T_r)]/T$	$H-H^{\circ}(T_r)$	$\Delta_f H^{\circ}$	$\Delta_f G^{\circ}$	log K_f
0	0.	0.	INFINITE	-10.186	35.927	35.927	INFINITE
100	33.276	202.563	271.168	-6.861	34.898	39.963	-20.874
200	34.385	225.852	243.325	-3.495	33.897	45.422	-11.863
250	35.593	233.649	240.634	-1.746	33.460	48.355	-10.103
298.15	36.974	240.034	240.034	0.	33.095	51.258	-8.980
300	37.029	240.262	240.034	0.068	33.083	51.371	-8.944

$$-\frac{(G^{\circ}(T)-H^{\circ}(0K))}{T} = -\frac{(G^{\circ}(T)-H^{\circ}(298.15K))}{T} + \frac{1000.(H^{\circ}(0)-H^{\circ}(289.15K))}{T}$$

Figure A.1: JANAF table representation used during the calculation of partition function for NO_2 molecule.

$$-\frac{(G^{\circ}(T)-H^{\circ}(0K))}{T} = RTln\left[\left(\frac{q^{\circ}(V,T)}{V}\right)\frac{k_bT}{P^{\circ}}\right] \tag{A.7}$$

$$\mu^{\circ}(T) = -\frac{(G^{\circ}(T) - H^{\circ}(0K))}{T} = -\frac{(G^{\circ}(T) - H^{\circ}(298.15K))}{T} + \frac{1000.(H^{\circ}(0) - H^{\circ}(289.15K))}{T} \tag{A.8}$$

After the input of all the values and performing the conversions using equation 3.7 as mentioned in section 3.2.4 the partition function for the nonlinear polyatomic molecule NO_2 at 273 K using JANAF table was; q(V,T)_NO_2(JANAF)= 422.60. More information about the calculation of partition function can be found here can be found here [17, 20]. All the ideal gas partition functions for the molecules (N_2O, N_2O_4, NO_2, NO, and O_2) calculated using JANAF table and equations from the book by Donald McQuarrie from (273-2073)K and 1bar pressure are tabulated here. The values of partition functions for the ideal gas molecules(N_2O, N_2O_4, NO_2, NO, and O_2) calculated using JANAF table and equations from the book by Donald McQuarrie at temperature (273-2073)K are represented in tables A.1 and A.2.

Table A.1: NO2 and O2 partition function values used as input to brick simulation, calculated using JANAF tables and the equations from the book by McQuarrie [17, 20].

Calculated partition functions as an input to brick				
	NO_2		O_2	
Temperature (K)	JANAF	McQuarrie	JANAF	McQuarrie
273	422.600	422.702	227.857	227.781
373	313.999	314.074	169.836	169.480
473	251.534	251.593	136.881	135.831
573	211.025	211.073	115.531	113.927
673	182.668	182.711	100.597	98.533
773	161.738	161.779	89.584	87.121
873	145.676	145.715	81.140	81.308
973	132.976	133.014	74.467	74.319
1073	122.694	122.731	69.069	68.633
1173	114.207	114.244	64.618	63.916
1273	107.090	107.127	60.887	59.940
1373	101.042	101.079	57.719	56.544
1473	95.842	95.879	54.998	55.081
1573	91.328	91.365	52.637	52.519
1673	87.375	87.412	50.571	50.263
1773	83.887	83.924	48.751	48.262
1873	80.788	80.826	47.134	46.474
1973	78.020	78.058	45.692	44.868
2073	75.532	75.571	44.397	43.416

Table A.2: NO,N2O and N_2O_4 partition function values used as input to brick simulation, calculated using JANAF tables and the equations from the book by McQuarrie [17, 20].

Calculated partition functions as an input to brick						
	NO		N_2O		N_2O_4	
Temperature (K)	JANAF	McQuarrie	JANAF	McQuarrie	JANAF	McQuarrie
273	287.078	286.510	497.904	497.357	859.783	859.542
373	213.849	213.258	368.472	367.810	636.154	635.959
473	171.731	171.125	294.000	293.231	507.617	507.451
573	144.414	143.795	245.687	244.818	424.336	424.187
673	125.286	124.657	211.851	210.894	366.091	365.962
773	111.161	110.525	186.867	185.827	323.147	323.034
873	100.315	99.673	167.685	166.567	290.228	290.126
973	91.735	91.087	152.509	151.318	264.228	264.136
1073	84.783	84.130	140.216	138.956	243.201	243.118
1173	79.041	78.384	130.063	128.740	225.867	225.790
1273	74.223	73.563	121.545	120.161	211.348	211.278
1373	70.125	69.461	114.301	112.859	199.024	198.959
1473	66.599	65.933	108.070	106.574	188.443	188.382
1573	63.537	62.867	102.657	101.110	179.268	179.211
1673	60.852	60.180	97.914	96.318	171.244	171.190
1773	58.482	57.808	93.727	92.084	164.173	164.123
1873	56.375	55.698	90.006	88.318	157.901	157.854
1973	54.491	53.812	86.678	84.947	152.304	152.259
2073	52.797	52.116	83.687	81.915	147.282	147.240

B

Appendix-B

Table B.1: Calculated values for μ° or G° in kj/mol at (1 bar) reference pressure P° used as an input for Matlab code.

Temperature (K)	μ° NO	μ° O_2	$\mu^\circ NO_2$	$\mu^\circ N_2O$	$\mu^\circ N_2O_4$
273	-675.539	-541.115	-983.152	-1154.08	-1975.49
373	-696.852	-560.354	-1007.45	-1176.38	-2006.54
473	-718.968	-581.915	-1032.81	-1199.82	-2039.92
573	-741.744	-604.138	-1059.09	-1224.22	-2075.34
673	-765.055	-626.908	-1086.14	-1249.45	-2112.51
773	-788.843	-650.169	-1113.9	-1275.41	-2151.29
873	-813.053	-673.866	-1142.31	-1302.06	-2191.53
973	-837.646	-697.955	-1171.29	-1329.31	-2233.1
1073	-862.587	-722.402	-1200.81	-1357.13	-2275.9
1173	-887.848	-747.178	-1230.82	-1385.46	-2319.81
1273	-913.407	-772.257	-1261.28	-1414.28	-2364.78
1373	-939.241	-797.619	-1292.18	-1443.54	-2410.71
1473	-965.333	-823.243	-1323.47	-1473.23	-2457.56
1573	-991.668	-849.116	-1355.13	-1503.31	-2505.26
1673	-1018.23	-875.222	-1387.15	-1533.76	-2553.77
1773	-1045.01	-901.55	-1419.5	-1564.57	-2603.04
1873	-1072	-928.086	-1452.17	-1595.72	-2653.03
1973	-1099.17	-954.823	-1485.14	-1627.18	-2703.71
2073	-1126.54	-981.751	-1518.39	-1658.94	-2755.04

C

Appendix-C

Table C.1: Mole fraction results for NO_2, N_2O, O_2, N_2O_4 and NO at 1 bar pressure and (273-2073)K temperature from NPT-RXMC simulations in brick.

Mole fractions from Brick simulations at 1 bar

Temperature (K)	O_2	NO	NO_2	N_2O	N_2O_4
273	0.31735	0	0.07872	0.06862	0.53531
373	0.22347	0	0.68239	0.05224	0.04189
473	0.55849	0.00057	0.15014	0.29077	0.00004
573	0.58541	0.00535	0.10106	0.30818	0
673	0.59155	0.02549	0.07652	0.30644	0
773	0.58046	0.07798	0.05864	0.28292	0
873	0.55154	0.1698	0.04351	0.23514	0
973	0.51009	0.28873	0.03074	0.17044	0
1073	0.47049	0.39921	0.02071	0.10958	0
1173	0.44041	0.48214	0.01381	0.06365	0
1273	0.42255	0.53207	0.00922	0.03616	0
1373	0.41266	0.56009	0.00641	0.02084	0
1473	0.40753	0.57513	0.00461	0.01273	0
1573	0.40444	0.58427	0.00346	0.00782	0
1673	0.40277	0.58947	0.00266	0.0051	0
1773	0.40181	0.59262	0.0021	0.00348	0
1873	0.40123	0.59464	0.00166	0.00247	0
1973	0.40078	0.59622	0.00132	0.00168	0
2073	0.40051	0.5973	0.00103	0.00116	0

Table C.2: Mole fraction results for NO_2, N_2O, O_2, N_2O_4 and NO at 1 bar pressure and (273-2073)K temperature from Gibbs minimization simulations in MATLAB.

Mole fractions from MATLAB simulations at 1 bar

Temperature (K)	O_2	NO	NO_2	N_2O	N_2O_4
273	0.29164	0.0000	0.09978	0.04810	0.56048
373	0.51362	0.0000	0.22380	0.25919	0.00337
473	0.56242	0.0006	0.14347	0.29352	0.00003
573	0.58450	0.0054	0.10256	0.30752	0
673	0.59062	0.0259	0.07784	0.30568	0
773	0.57965	0.0785	0.05960	0.28219	0
873	0.55047	0.1715	0.04416	0.23389	0
973	0.50964	0.2894	0.03104	0.16993	0
1073	0.46980	0.4007	0.02088	0.10867	0
1173	0.44034	0.4822	0.01385	0.06356	0
1273	0.42237	0.5323	0.00932	0.03596	0
1373	0.41250	0.5604	0.00647	0.02063	0
1473	0.40723	0.5758	0.00466	0.01232	0
1573	0.40436	0.5844	0.00348	0.00773	0
1673	0.40275	0.5895	0.00268	0.00508	0
1773	0.40181	0.5926	0.00212	0.00349	0
1873	0.40123	0.5945	0.00173	0.00250	0
1973	0.40086	0.5959	0.00143	0.00185	0
2073	0.40062	0.5968	0.00121	0.00141	0

Table C.3: Mole fraction results for NO_2, N_2O, O_2, N_2O_4 and NO at 10 bar pressure and (273-2073)K temperature from NPT-RXMC simulations in brick.

Mole fractions from Brick simulations at 10 bar

Temperature (K)	O_2	NO	NO_2	N_2O	N_2O_4
273	0.34289	0	0.00778	0.08247	0.56252
373	0.41543	0.00659	0.37125	0.09891	0.10782
473	0.41162	0.00024	0.39752	0.18778	0.00285
573	0.54847	0.00289	0.16554	0.28306	0.00004
673	0.56556	0.01395	0.12877	0.29171	0
773	0.56826	0.04391	0.10322	0.28461	0
873	0.55692	0.10149	0.08219	0.2594	0
973	0.53254	0.18613	0.06439	0.21694	0
1073	0.50257	0.28256	0.04784	0.16703	0
1173	0.47253	0.37409	0.03483	0.11855	0
1273	0.44773	0.44817	0.02514	0.07896	0
1373	0.43064	0.49932	0.01838	0.05165	0
1473	0.41914	0.53387	0.01375	0.03324	0
1573	0.41219	0.55538	0.01052	0.02192	0
1673	0.4079	0.56923	0.00811	0.01476	0
1773	0.40528	0.57777	0.00658	0.01037	0
1873	0.40364	0.58348	0.00537	0.00751	0
1973	0.40264	0.58725	0.00445	0.00567	0
2073	0.40187	0.59004	0.00379	0.0043	0

Table C.4: Mole fraction results for NO_2, N_2O, O_2, N_2O_4 and NO at 10 bar pressure and (273-2073)K temperature from Gibbs minimization simulations in MATLAB.

Mole fractions from MATLAB simulations at 10 bar

Temperature (K)	O_2	NO	NO_2	N_2O	N_2O_4
273	0.24748	0	0.03874	0.00206	0.71173
373	0.42909	0.00001	0.31383	0.19406	0.06300
473	0.51300	0.00029	0.22704	0.25894	0.00073
573	0.54741	0.00285	0.16738	0.28233	0.00003
673	0.56436	0.01396	0.13081	0.29086	0
773	0.56735	0.04398	0.10471	0.28395	0
873	0.55622	0.10165	0.08327	0.25886	0
973	0.53257	0.18597	0.06445	0.21701	0
1073	0.50195	0.28347	0.04826	0.16632	0
1173	0.47172	0.37547	0.03525	0.11756	0
1273	0.44723	0.44883	0.02553	0.07841	0
1373	0.43001	0.50051	0.01863	0.05085	0
1473	0.41893	0.53423	0.01386	0.03299	0
1573	0.41210	0.55555	0.01055	0.02180	0
1673	0.40791	0.56902	0.00823	0.01483	0
1773	0.40532	0.57769	0.00658	0.01042	0
1873	0.40368	0.58340	0.00537	0.00755	0
1973	0.40261	0.58729	0.00447	0.00564	0
2073	0.40189	0.59000	0.00378	0.00432	0

Appendix-D

In this section some setbacks from the NPT-reaction ensemble simulations are discussed. Before simulating the bulk equilibrium reactions 3.3, 3.4, 3.5 as mentioned in section 3.2, simulations were performed in brick for the following set of reactions 3.4, 3.5, D.1 at 1 bar pressure and 273 K - 1873 k temperature.

$$N_2 + O_2 \rightleftharpoons 2\,NO \tag{D.1}$$

For these simulations, the number of molecules for N_2, N_2O, NO_2, NO, and O_2 were set to 150, 130, 110, 110, and 80. The results from these simulations are shown if figure D.1

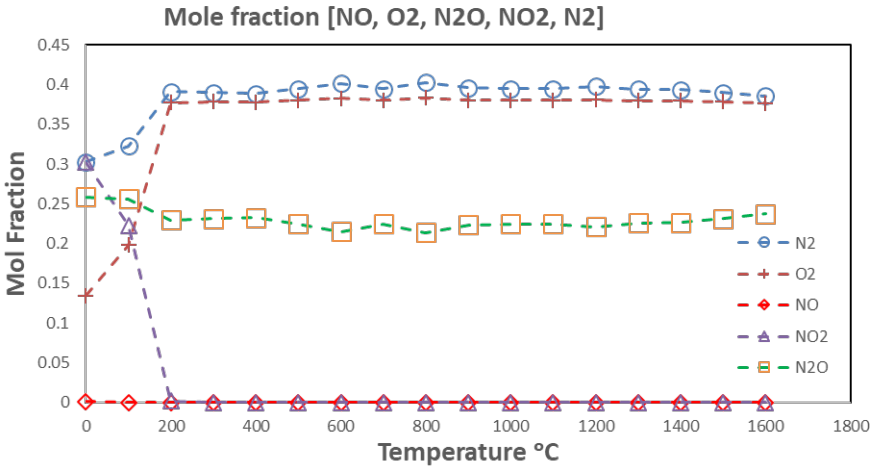

Figure D.1: The Mole fractions results of NO_2, N_2O, O_2, N_2, and NO at 1 bar pressure and $0°C$ to 1800 $°C$ or (273-2073)K temperature, computed using NPT-RXMC ensemble simulations in BricK for the reactions 3.4, 3.5, and D.1.

In figure D.1, one can observe the mole fraction of N_2 and O_2 is higher and constant till 1873 K temperature. But this doesn't seem right. The mole fraction of NO should start increasing, whereas the mole fraction of N_2 and O_2 should start decreasing at a temperature above 773 K (see section 4.3). But this was not the case here. Even the mole fraction of N_2O, which should decrease after 773 K, was not decreasing and was constant till 1873 K temperature. Similarly,

the mole fraction of NO was also zero, which should not happen and NO_2 mole fraction, which starts decreasing after 773 K. In this case, it reduced to zero at 473K. This was also a problem. In order to identify the problem, the best method was to calculate the Standard Gibbs free energy of all the four reactions 3.3, 3.4, 3.5, and D.1 and check if all four reactions were spontaneous, exergonic and favored reaction products rather than reactants. This was done in three different ways. The first way was to calculate standard reference chemical potential $\mu^{\circ}(T)$ as shown in equation D.2

$$\mu^{\circ}(T) - E^{\circ}(0K) = -RTln\left[\left(\frac{q^{\circ}(V,T)}{V}\right)\frac{k_bT}{P^{\circ}}\right] \tag{D.2}$$

For a pure component, $\mu^{\circ} = G^{\circ}$, and E_0 the standard molar enthalpy of a molecule at T=0 K equal to -D_0, the atomization energy. And in this way the partitions functions were used here to calculate the standard reference Gibbs free energy of all the four reactions 3.3, 3.4, 3.5, and D.1. The second way was, by checking the spontaneity of reactions which is given by equation D.3

$$G = H - TS \tag{D.3}$$

Here G is the Gibbs free energy, H is the enthalpy, and S is the entropy. And the standard reference Gibbs free energy is given by equation D.4

$$\Delta^{\circ}G = \Delta^{\circ}H - T\Delta^{\circ}S \tag{D.4}$$

For the standard reference, Gibbs free energy given by equation D.4, the standard reference enthalpy values, and the standard reference entropy values in equation D.4 for different components involved in the reactions were taken from the JANAF tables[19]. The last method was to calculate the standard reference Gibbs free energy for all the reactions 3.3, 3.4, 3.5, and D.1 using equation D.5. The values for reactants and products for various components involved in the reaction were taken from JANAF tables[19].

$$\Delta^{\circ}G = \sum Products - \sum Reactants. \tag{D.5}$$

Using equation D.2, D.4, and D.5 the standard reference Gibbs free energy for all the reactions 3.3, 3.4, 3.5, and D.1 was calculated and the results are tabulated in tables D.1, D.2, D.3, and D.4.

Table D.1: standard reference Gibbs free energy for the reaction 3.3 calculated using equations D.2, D.4, and D.5.

$N_2O_4 = 2NO_2$, 3.3			
Temperature (K)	$\Delta^\circ G$ calculated using partition function equation D.2 in KJ/mol	$\Delta^\circ G$ calculated using JANAF tables, and equation D.5 KJ/mol	$\Delta^\circ G$ calculated using JANAF tables, and equation D.4 KJ/mol
273	8.17762468	8.963	9.154
373	-9.421513988	-8.7225	-8.4156
473	-26.82158932	-26.066	-25.985
573	-44.00538035	-43.182	-43.55
673	-60.98263034	-60.105	-61.125
773	-77.76870928	-76.883	-78.695

Table D.2: standard reference Gibbs free energy for the reaction 3.4 calculated using equations D.2, D.4, and D.5.

$2NO + O_2 = 2NO_2$, 3.4			
Temperature (K)	$\Delta^\circ G$ calculated using partition function equation D.2 in KJ/mol	$\Delta^\circ G$ calculated using JANAF tables, and equation D.5 KJ/mol	$\Delta^\circ G$ calculated using JANAF tables, and equation D.4 KJ/mol
273	-77.32582473	-74.18	-74.361
373	-63.6425363	-59.28	-59.702
473	-49.69197078	-44.21	-45.042
573	-35.62467412	-28.994	-30.38
673	-21.51572232	-13.718	-15.72
773	-7.402226538	-1.583	-1.064

Table D.3: standard reference Gibbs free energy for the reaction 3.5 calculated using equations D.2, D.4, and D.5.

$3NO = N_2O + NO_2$,3.5			
Temperature (K)	Δ°G calculated using partition function equation D.2 in KJ/mol	Δ°G calculated using JANAF tables, and equation D.5 KJ/mol	Δ°G calculated using JANAF tables, and equation D.4 KJ/mol
273	-105.5411337	-108.47	-108.69
373	-85.49159652	-91.0035	-91.466
473	-64.82385936	-73.443	-74.239
573	-43.69954145	-55.7985	-57.0124
673	-22.21076694	-38.15275	-39.78
773	-0.416115371	-20.5322	-22.558

Table D.4: standard reference Gibbs free energy for the reaction D.1 calculated using equations D.2, D.4, and D.5.

$N_2+O_2 = 2NO$, D.1			
Temperature (K)	Δ°G calculated using partition function equation D.2 in KJ/mol	Δ°G calculated using JANAF tables, and equation D.5 KJ/mol	Δ°G calculated using JANAF tables, and equation D.4 KJ/mol
273	178.1875571	173.793	173.82
373	176.2611843	171.286	171.34
473	174.8370081	168.78	168.87
573	173.4170893	166.27	166.39
673	171.9990457	163.75	163.91
773	170.5806578	161.236	161.44

From the table D.1, D.2, D.3 it can be found for reactions 3.3, 3.4, and 3.5 the standard reference Gibbs free energy of reaction ($\Delta°G < 0$) and hence all the three reactions 3.3, 3.4, and 3.5 are spontaneous and exergonic and favours products formation. But in case of reaction D.1 and from table D.4 one can observe the standard reference Gibbs free energy of reaction ($\Delta°G > 0$) and hence the reaction is non-spontaneous and endorgonic and favours reactants production. Hence it was difficult to simulate all four reactions 3.3, 3.4, 3.5, and D.1. It was also found from literature, that reaction D.1 initiates at temperature above 2000 K[25]. And as per the operating conditions provided by the Nitric acid production facility the tail gas was at 773 K temperature. Hence the reaction D.1 was neglected and was not considered for the bulk phase reaction equilibrium NPT-RXMC simulations.

Bibliography

[1] asia.iza structure.org. Database of zeolite structures. URL http://asia.iza-structure.org/IZA-SC/framework_3d.php?STC=FAU.

[2] Peng Bai, Michael Tsapatsis, and J Ilja Siepmann. Trappe-zeo: Transferable potentials for phase equilibria force field for all-silica zeolites. The Journal of Physical Chemistry C, 117(46):24375–24387, 2013.

[3] Emeric Bourasseau, Veronique Lachet, Nicolas Desbiens, Jean-Bernard Maillet, Jean-Marie Teuler, and Philippe Ungerer. Thermodynamic behavior of the co2+ no2/n2o4 mixture: a monte carlo simulation study. The Journal of Physical Chemistry B, 112(49): 15783–15792, 2008.

[4] Jing Chao, Randolph C Wilhoit, and Bruno J Zwolinski. Gas phase chemical equilibrium in dinitrogen trioxide and dinitrogen tetroxide. Thermochimica Acta, 10(4):359–371, 1974.

[5] clariant.com. Advanced zeolite material. URL https://www.clariant.com/en/Solutions/Products/2019/04/24/08/20/Faujasite-Zeolites-FAU.

[6] Asit K Das, Juray De Wilde, Geraldine J Heynderickx, Guy B Marin, Steen B Iversen, and Karsten Felsvang. Simultaneous adsorption of so2 nox from flue gases in a riser configuration. AIChE journal, 47(12):2831–2844, 2001.

[7] D Dubbeldam, S Calero, D Ellis, and R Snurr. Raspa 2.0: Molecular software package for adsorption and diffusion in (flexible) nanoporous materials, 2015. DOI, 10(08927022.2015): 1010082.

[8] Dieter Förtsch. An engineering approach for estimating the formation of nitric oxide from fuel-nitrogen. Chemical Engineering & Technology, 42(11):2428–2433, 2019.

[9] Volker Gramlich. Untersuchung und verfeinerung pseudosymmetrischer strukturen. PhD thesis, ETH Zurich, 1971.

[10] Niels Hansen, Felix AB Agbor, and Frerich J Keil. New force fields for nitrous oxide and oxygen and their application to phase equilibria simulations. Fluid Phase Equilibria, 259 (2):180–188, 2007.

[11] Remco Hens, Ahmadreza Rahbari, Sebastián Caro-Ortiz, Noura Dawass, Máté Erdős, Ali Poursaeidesfahani, Hirad Salehi, Alper Celebi, Mahinder Ramdin, Othonas A Moultos, et al. Brick-cfcmc: open source software for monte carlo simulations of phase and reaction equilibria using the continuous fractional component method. Journal of Chemical Information and Modeling, 2020.

[12] JA Hriljac, MM Eddy, AK Cheetham, JA Donohue, and GJ Ray. Powder neutron diffraction and 29si mas nmr studies of siliceous zeolite-y. Journal of Solid State Chemistry, 106 (1):66–72, 1993.

[13] Muhammad Shahzad Kamal, Shaikh A Razzak, and Mohammad M Hossain. Catalytic oxidation of volatile organic compounds (vocs)–a review. Atmospheric Environment, 140: 117–134, 2016.

[14] B Marler. Silica-zsm-22: synthesis and single crystal structure refinement. Zeolites, 7(5): 393–397, 1987.

[15] I Matito-Martos, Ana Martin-Calvo, JJ Gutierrez-Sevillano, M Haranczyk, M Doblare, JB Parra, CO Ania, and S Calero. Zeolite screening for the separation of gas mixtures containing so 2, co 2 and co. Physical Chemistry Chemical Physics, 16(37):19884–19893, 2014.

[16] I Matito-Martos, A Rahbari, A Martin-Calvo, D Dubbeldam, TJH Vlugt, and S Calero. Adsorption equilibrium of nitrogen dioxide in porous materials. Physical Chemistry Chemical Physics, 20(6):4189–4199, 2018.

[17] Donald Allan McQuarrie and John Douglas Simon. Physical chemistry: a molecular approach, volume 1. University science books Sausalito, CA, 1997.

[18] Russell E Morris, Scott J Weigel, Neil J Henson, Lucy M Bull, Michael T Janicke, Bradley F Chmelka, and Anthony K Cheetham. A synchrotron x-ray diffraction, neutron diffraction, 29si mas-nmr, and computational study of the siliceous form of zeolite ferrierite. Journal of the American Chemical Society, 116(26):11849–11855, 1994.

[19] nist.gov. Nist-janaf thermochemical tables, . URL https://janaf.nist.gov/.

[20] nist.gov. Computational chemistry comparison and benchmark data base, . URL https://cccbdb.nist.gov/exp1x.asp.

[21] J Pérez-Ramırez, F Kapteijn, K Schöffel, and JA Moulijn. Formation and control of n2o in nitric acid production: where do we stand today? Applied Catalysis B: Environmental, 44(2):117–151, 2003.

[22] Ali Poursaeidesfahani, Remco Hens, Ahmadreza Rahbari, Mahinder Ramdin, David Dubbeldam, and Thijs JH Vlugt. Efficient application of continuous fractional component monte carlo in the reaction ensemble. Journal of chemical theory and computation, 13(9): 4452–4466, 2017.

[23] A Rahbari. Thermodynamics of Industrially Relevant Systems: Method Development and Applications. PhD thesis, Delft University of Technology, 2020.

[24] Dave S Reay, Eric A Davidson, Keith A Smith, Pete Smith, Jerry M Melillo, Frank Dentener, and Paul J Crutzen. Global agriculture and nitrous oxide emissions. Nature climate change, 2(6):410–416, 2012.

[25] William F Schneider. 10 fundamental concepts in molecular simulation of nox catalysis. 2005.

[26] Cory M Simon, Berend Smit, and Maciej Haranczyk. pyiast: Ideal adsorbed solution theory (iast) python package. Computer Physics Communications, 200:364–380, 2016.

[27] Joseph Mauk Smith. Introduction to chemical engineering thermodynamics, 1950.

[28] Lijuan Song and Lovat VC Rees. Adsorption and diffusion of cyclic hydrocarbon in mfi-type zeolites studied by gravimetric and frequency-response techniques. Microporous and Mesoporous Materials, 35:301–314, 2000.

[29] Weizhen Sun, Li-Chiang Lin, Xuan Peng, and Berend Smit. Computational screening of porous metal-organic frameworks and zeolites for the removal of so2 and nox from flue gases. AIChE Journal, 60(6):2314–2323, 2014.

[30] Teruoki Tago, Daichi Aoki, Kazuyuki Iwakai, and Takao Masuda. Preparation for size-controlled mor zeolite nanocrystal using water/surfactant/organic solvent. Topics in Catalysis, 52(6-7):865–871, 2009.

[31] Optimization Toolbox. Users guide, the mathworks. Inc.: Natick, MA, USA, 2010.

[32] H Van Koningsveld, H Van Bekkum, and JC Jansen. On the location and disorder of the tetrapropylammonium (tpa) ion in zeolite zsm-5 with improved framework accuracy. Acta Crystallographica Section B: Structural Science, 43(2):127–132, 1987.

[33] Thijs JH Vlugt, Jan PJM Van der Eerden, Marjolein Dijkstra, Berend Smit, and Daan Frenkel. Introduction to molecular simulation and statistical thermodynamics. http://homepage. tudelft. nl/v9k6y/imsst/index. html, 2009.

[34] Yanan Wang, Yang Gao, Weifeng Chu, Dongpu Zhao, Fucun Chen, Xiangxue Zhu, Xiujie Li, Shenglin Liu, Sujuan Xie, and Longya Xu. Synthesis and catalytic application of fer zeolites with controllable size. Journal of materials chemistry A, 7(13):7573–7580, 2019.

[35] Hu Yang, Zhenghua Ping, Guoxin Niu, Huiwen Jiang, and Yingcai Long. Tg/dtg/dta study on interaction between the framework of high silica hydrophobic fau zeolite and adsorbed organics. Langmuir, 15(16):5382–5388, 1999.

[36] J-H Yun, Y He, M Otero, T Düren, and NA Seaton. Adsorption equilibrium of polar/non-polar mixtures on mcm-41: experiments and monte carlo simulation. In Studies in Surface Science and Catalysis, volume 144, pages 685–692. Elsevier, 2002.

[37] zeoplusplus.org. Zeo++. URL http://zeoplusplus.org/.